Heliyon 10 (2024) e24000

Contents lists available at ScienceDirect

Heliyon

journal homepage: www.cell.com/heliyon

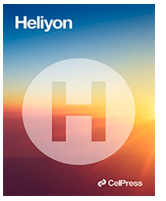

Techno-economic and environmental analysis of a hybrid PV/T solar system based on vegetable and synthetic oils coupled with TiO_2 in Cameroon

Armel Zambou Kenfack [a,*], Modeste Kameni Nematchoua [a], Elie Simo [a], Franck Armel Talla Konchou [b], Mahamat Hassane Babikir [c], Boris Abeli Pekarou Pemi [a], Venant Sorel Chara-Dackou [a,d]

[a] Energy and Environment Laboratory, Department of Physics, Faculty of Science, University of Yaoundé I, P.O. Box 812, Cameroon
[b] Department of Physics, University Institute of Technology Fotso Victor of Bandjoun (IUT-FV), Bandjoun, P.O. Box 134, Cameroon
[c] Department of Physics, Faculty of Science, University of Ndjamena, Ndjamena, P.O. Box 1117, Chad
[d] Carnot Energy Laboratory(CEL), Department of Physics, Faculty of Science, University of Bangui, P.O. Box 1450, Bangui, Central African Republic

ARTICLE INFO

Keywords:
Energy/exergy analysis
Vegetable/synthetic oils
Photovoltaic/thermal systems
Technical-economic analysis
Environmental analysis
Multi-objective method

ABSTRACT

To assess the production potential, economic profitability and ecobalance of the photovoltaic/thermal (PV/T) system in Cameroon, different configurations of HTF based on water, vegetable and synthetic oils, coupled with different forms of titanium dioxide (TiO_2) are used. A numerical code is written in Matlab. The PV/T model connected in direct contact PV-absorber is validated and a multi-objective optimization of the system is performed. The hourly evolution of PV cell temperature for the six HTF configurations revealed a value below 36 °C with Coton/TiO_2. The platelets-and spherical-shaped nanoparticles increase the convection transfer coefficient between the fluids and the tubes. TiO_2 showed a higher thermal influence in vegetable and synthetic oils than in water at a volume concentration of 4 %. The cotton/TiO_2 configuration showed a 12.08 % improvement in electrical efficiency over conventional PV systems with low exergy efficiency compared to water. Configurations with therminolVP-1/TiO_2 are better, with the proposed energy cost reduced to 33 % of the price of electricity in Cameroon. The PV/T-Palm/TiO_2 system showed an energy cost of $0.03 with a net present value of $568.45, an emission rate of 7.78 kg, a reversibility index of 1.95, an annual cost of $7.07 and a payback time of 5.97yr. This shows that PV/T systems based on vegetable oils are economical.

1. Introduction

Cameroon is a country in the sub-Saharan zone with annual solar radiation estimated between 1400 and 2200 kWh/m_2/year with a very growing population estimated at around 27 million inhabitants and with an area of 475,442 km^2 [1]. Since 2020, this country has experienced high inplateletsion linked to the Covid-19 pandemic and recently the Russo-Ukrainian conflict. The cost of electrical energy has recently increased and its average is $0.33/kWh. Less than 14 % of rural households and 57 % in urban areas are connected to the national electricity grid [2]. In other words, 80 % of the population does not have continuous access to electricity [3]. To remedy

* Corresponding author.
E-mail address: armelzambou199@gmail.com (A.Z. Kenfack).

https://doi.org/10.1016/j.heliyon.2024.e24000
Received 25 September 2023; Received in revised form 24 December 2023; Accepted 2 January 2024
Available online 6 January 2024
2405-8440/© 2024 The Authors. Published by Elsevier Ltd. This is an open access article under the CC BY license (http://creativecommons.org/licenses/by/4.0/).

this situation, several photovoltaic solar power plants are being developed, such as the recent one in Guider in North Cameroon with a planned nominal power of 15 MW. But one of the problems encountered with Photovoltaic (PV) panels is the heating of the cells, which until now only produce an electrical power of approximately 30 % of that expected with the advent of tandem cells, of which manufacturing processes are still complex and purchasing and installation costs are not very accessible. According to several studies, the efficiency of PV module drops up to 0.08 % with increased temperature of PV cells [4]. One of the optimization methods most used today to increase the performance of the PV module is PV/T hybridization (Photovoltaic and Thermal). Below the PV module, a thermal collector is attached to recover heat from the PV cells [5,6]. In this system and depending on the type, fluids such as air, water, vegetable or synthetic oils and nanofluids. These techniques are active methods used to absorb this heat and produce thermal energy [7–9]. But the multiplicity of its transfer fluids requires an in-depth comparative study to make it possible to choose an optimal fluid for PV/T systems. Therefore, electricity generation is significantly improved [10,11].

Mishra and Tiwari [12] carried out a comparative study on two types of water PV/T models. One half and the other completely covered by the PV. Their study showed a significant improvement in the performance of the half-covered system compared to the fully covered PV system. This is due to the high thermal output of half-covered PV. Their study could be improved by considering the gap between the PV and the absorber. Moreover, the PV/T model directly connected PV-absorber requires an economic analysis. A feasibility study on a PV system based on techno-economic and environmental analysis established that solar PV systems are eco-environmental and profitable [13]. Their analysis being based on some aspect such as energy cost, efficiency factor, capacity factor and payback time [14] which could have been more conclusive considering indicators such as sustainability index of the system which is affected by cell temperature and other factors. In addition, the proposed system with one or two axis tracking operates with a high cell temperature which causes considerable exergy losses during the day which can be more efficient thanks to the HTF.

Several numerical and experimental studies have been carried out with different cooling fluids. The authors [15] demonstrated that a water-cooled and nanofluid PVT system can reduce the panel temperature by 10 °C and 20 °C respectively. This parameter is also influenced by the temperature of the inlet fluid which strongly depends on climatic conditions [16].

Further, In order to choose an optimal nanoparticle, a selective study on three types of nanoparticles Al_2O_3, TiO_2, ZnO based on water for PV/T hybridization in climatic conditions of Iran [17]. Their model, based on an analytical hierarchical process, showed that PV/T-ZnO is more efficient both thermally and electrically with a reduction of CO_2 85.8 kg. On the other hand, it TiO_2 was the element very effectively close to zinc dioxide. Its preparation, for nanofluids, involves the production of solid particles of nanometric size, followed by their dispersion in base fluids. This step is crucial to obtain stable and cost-effective nanofluids with improved thermo-physical properties. Synthesis methods and important physical properties, such as thermal conductivity and viscosity, must be carefully considered when preparing nanofluids based on TiO_2 desired applications [18].

However, a similar study allowing a comparison on several types of basic fluids is missing in the literature. Several studies have shown a relationship between the flow rate of these fluids and the performance of the PV system [19,20]. The authors [21] noted the fact that simultaneous cooling of the PV/T system with a very high flow rate considerably increases the overall efficiency compared to a low flow rate, when solar radiation is maximum (1050 W/m^2). This is also the case with nanofluids [22]. However, studies of PV/T systems with existing nanofluids do not highlight the base fluid requiring a very small nanoparticle concentration. As exergy is the part of energy that can be directly converted into useful energy [23], a systems analysis taking this parameter into consideration is very necessary. The authors [24] carried out extensive tests carried out on the glass-PV and glass-PV-glass collector. Their study taking into account the exergy losses on the two configurations revealed that the PV/T system with a double layer in front and behind the PV significantly improves the performance of the system. Other cooling fluids are explored in the literature. Tests have been carried out with vegetable and synthetic oils. A characterization of vegetable and synthetic oils shows that they have very good characteristics to be an alternative to water in solar systems [25,26]. The stability of nanofluids based on vegetable oils is demonstrated in some subsequent studies. **Fazlay et al.** [27] used soybean oil combined with Mxene (Ti_3C_2) for a PV/T solar system compared to the Mxene/palm nanofluid. It emerges from their study that the best system is the PV/T-Mxene/Soyabean with a flow rate of 0.07 kg/s, which made it possible to increase the electrical power by 15.44 % with a reduction in the temperature on the surface of the 14 °C sensor. However, the effect of nanoparticle morphology as well as exergy performance were not taken into account. Furthermore, a comparative study presenting the effect of each NP with different types of base fluids is not presented and the effect of the thermo-physical properties of these oils on the electrical consumption of the pump is not also evaluated in the previous studies. A thermo-physical evaluation of three types of vegetable oils including coconut, soybean and palm oil suspended with hybrid nanoparticles was carried out by **Vignesh et al.** [28]; Among these fluids, palm oil-based NFs were found to have better thermophysical properties. However, a study over an annual period and not just a daily period of these nanofluids based on vegetable oils could be very conclusive. The comparison carried out between water and Therminol VP1 as base fluid with the addition of nanoparticles Al_2O_3 and CuO showed that the nanoparticles have more efficiency in Therminol VP1 than in water [29]. It is therefore necessary to search for an appropriate optimization method that takes into account several improvement factors.

The LCA (Life Cycle Energy Analysis) approach and LCEA (Life Cycle Exergy Analysis) approach method are respectively used to evaluate the cumulative energy consumption and exergy expended throughout the life cycle of the PV/T system by the authors [30]. Their studies reveal that the use of nanofluids can avoid emissions of approximately 448 kg of CO_2 eq/m^2/year. However, the temperature of the glass collector and the effect of the electrical pumping power have a certain sensitivity that should not be neglected on performance. A techno-economic and environmental analysis with a one-dimensional finite difference model revealed an attenuation of 6.9 tonnes and 6.4 tonnes of C O_2 for copper oxide and alumina nanoparticles respectively with a lifetime of up to 30 years in areas with high sunlight [31]. Similar studies show the technical-economic feasibility of PV/T-Ag/water systems with a total investment rate of 686.35 USD and a discount rate of 2 % [32]. Abdo and Saidani [33] used saturated alumina hydrogels at a concentration of 0.5 % for higher performance of the PV/T sensor, but lower costs were obtained with a concentration of 0.25 % nanoparticles at 1000W/m^2. The

environmental analysis revealed a reduced annual CO_2 emission of up to 7.95 tonnes for a farm of 100 m^2.

The observation made from previous studies is that the cooling of the PV/T system which will be adopted will certainly depend on the improvement of efficiency, its reliability, costs and its impact on the environment. Several previous studies are done with the PV/T model which leaves an air gap between the back of the PV module and the absorber. In addition, generally constant during simulations, no study takes into account the shape of nanoparticles in several types of basic fluid on the performance of the PV/T system. Multi-objective optimization which is an artificial intelligence method has not yet been fully explored for improving the performance of solar PV/T systems; A very limited number of research deals with the technical-economic and environmental evaluation of vegetable and synthetic oils in comparison with two types of water (natural and mineral) in a hybrid PV/T system. In addition to this, the evaluation among nanofluids, of the base fluid requiring a very small concentration of nanoparticles which are expensive has not been the subject of any study. Of all these, no similar study has yet been carried out in a sub-Saharan country.

This study aims to carry out an optimal selection of optimal cooling fluid thanks to a PV/T model connected in direct PV-absorber contact to evaluate the production potential and the economic and environmental profitability of the system in the climatic zones of the Cameroon. Thus, a mathematical modeling of the PV/T solar system in direct PV-absorber contact is proposed. Six configurations of HTFs (untreated water, treated water, therminolVP-1, therminol 66, cottonseed oil and palm oil) coupled with titanium dioxide TiO_2 are evaluated to determine the $_{best}$ configuration of the PV/T system in five cities in the Cameroon. The results from this simulation are compared with those in the literature. The evaluation of nanoparticle morphology on the performance of the PV/T hybrid system are presented. Then, an analysis of the CO_2 emission for each scenario is presented. This with the aim of finding the optimal PV/T scenario. This study therefore has the following main contributions.

- ➢ The PV/T model in direct PV-absorber contact is validated with vegetable oils;
- ➢ The lamellar and spherical nanoparticles stood out significantly in terms of system performance;
- ➢ The annual electrical production of the cotton/TiO_2 system has a greater value in Maroua and synthetic and vegetable oils have more thermal influence in hot zones;
- ➢ The MOO method allowed us to have the optimal PV/T configurations for each zone;
- ➢ The cost of energy is better compared to the unit price in Cameroon with a lower environmental impact.

After this introduction which constitutes the first section, it will follow the second section which is the presentation of the study areas, followed by the third section devoted to the presentation of the hybrid PV/T solar system. The fourth section focuses on mathematical modeling. The environmental and economic models are presented in the fifth section. The sixth section presents the numerical model, then the seventh section devotes to the results and discussions.

2. Study areas

The use of multiple PV cell cooling fluid configurations depends on several climatic factors. Local meteorological and radiometric variabilities, such as solar radiation, ambient temperature and wind speed, play a key role in the performance of the hybrid PV/T solar system. For this study, the major tropical and equatorial climatic zones of Cameroon are selected. Two (2) representative cities (Maroua, N'Gaoundéré) are chosen in the tropical climatic zone and three (3) representative cities (Yaoundé, Douala and Bafoussam) are chosen in the equatorial climatic zone. Initially, the study is carried out in Yaoundé then extrapolated to the four other study areas. Geographic coordinates and some economic information considered differently are contained in Table 1. Note that these cities have several potentials, including agricultural potential [34,35].

3. Physical model

The PV/T hybrid solar system considered in this study is the one shown in Fig. 1 with its various thermal and electrical components. The heat is absorbed by the fluid from the cold storage tank passing below the PV collector using a pump and then stored in the hot tank. At a very high temperature in the hot tank, the heat passes into the exchanger where it is stored in the tank. Then the cold fluid returns to the cold tank and the process begins again. The electricity produced in turn is stored in storage batteries [32].Technical characteristics and other system sizing information are presented in Table 2-4.

Table 1
Geographic coordinates and economic parameters of cities.

Climatic zone	City	Altitude (m)	Latitude (North)	Longitude (East)	Inplateletsion rate (%)	Interest rate (%)
Tropical	Maroua	406	10.35°	14.18°	6.4	7.1
	N'Gaoundéré	1128	7.19°	13.35°	7.4	8.1
Equatorial	Yaounde	726	3.52°	11.31°	6.2	7.5
	Douala	13	4.02°	9.42°	5.7	6.01
	Bafoussam	1521	5.28°	10.25°	7.3	7.5

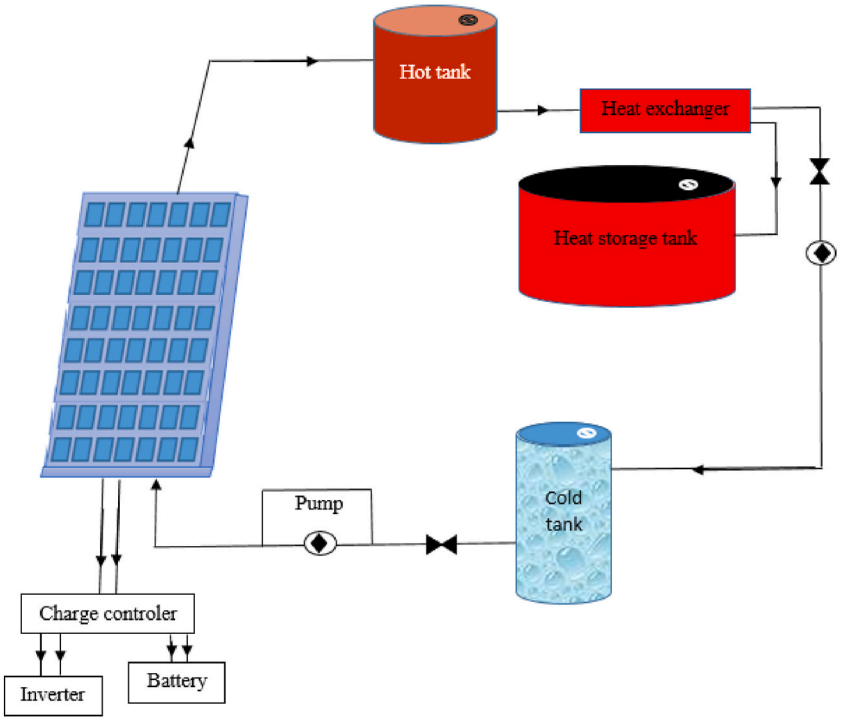

Fig. 1. Presentation of the physical model of the PV/T hybrid solar system.

Table 2
Calculation correlations of the thermophysical properties of nanofluids and the coefficients characteristic of the morphology of the nanoparticles [36,37,38,39].

Nanofluid

$\rho_{nf} = (1-\varphi)\rho_{fb} + \varphi\rho_{np}$

$K_{nf} = 0.25((3\varphi-1)K_{np} + (2-3\varphi)K_{bf} + ((3\varphi-1)K_{np} + (2-3\varphi)K_{np})^2 + 8K_{np}K_{bf})^{0.5}$

$Cp_{nf} = \left(\frac{\rho_{bf}}{\rho_{nf}}\right)(1-\varphi)Cp_{bf} + \varphi\left(\frac{\rho_{bf}}{\rho_{nf}}\right)Cp_{bf} = Cp_{bf}(1-x)^{-1}$

$\mu_{nf} = \mu_{bf}(1 + A_1\varphi + A_2\varphi^2)$

Coefficient	Blade	cylinder	Platelet	Brig
A_1	14.6	13.5	37.1	1.9
A_2	123.3	612.6	471.4	904.4

Nanosphere	Nanowire	Nanofilms
$x = \frac{2d}{D}$	$x = \frac{4d}{3l}$	$x = \frac{2d}{3h}$

Table 3
Unit price of basic fluids [25,40].

Fluid	Unit price
TH66	$20 USD/L
THVP-1	$15 USD/L
T.W.	$0.50 USD/ m^3
U.W.	$0.10 USD/ m^3
PA oil	$2 USD/L
CO oil	$1.5 USD/L

4. Mathematical modeling

The mathematical modeling of the hybrid PV/T solar system requires taking into account its optical, thermal and electrical aspects, of which Fig. 2 presents some of them. Thus several physical phenomena govern the system and intervene simultaneously in the operating process. When solar irradiation hits the glass layer, a slight part is reflected while a large part reaches the PV module. At the level of PV cells, the imbalance due to hole-electron recombination at the junctions gives rise to an electric field which during its movement creates a direct electric current. During the generation of this current, the PV cells heat up and part of the solar radiation also contributes to its heating which is therefore absorbed by the absorber plate. The tubes below the absorber plate recover this heat which, in turn, is transferred to the heat transfer fluid. The insulation underneath prevents energy loss to the rear to allow all excess

Table 4
PV/T system input parameters [4,38].

Rated power (Monocrystalline)	50W	K_{np}	8.9 W/mK
Kind	Monocrystalline	ρ_g	0.78 kg/ m^3
Nominal output (1000 W, 25 °C)	14 %		
HAS	1.3 m^2	ρ_{np}	4250 kg/ m^3
C_{np}	686 J/kg K	ρ_p	2707 kg/ m^3
C_g	670 J/kg K	ρ_t	8950 kg/ m^3
C_i	670 J/kg K	ρ_i	20kg/ m^3
D	5 nm	σ	1.38×10^{-23} m^2 kg. $s^{-2}K^{-1}$
D	0.256 nm	h	5.4 nm
L	6.7 nm	ε_g	0.88
K_i	0.034 W/m K	ε_p	0.05
K_g	310 W/mK		

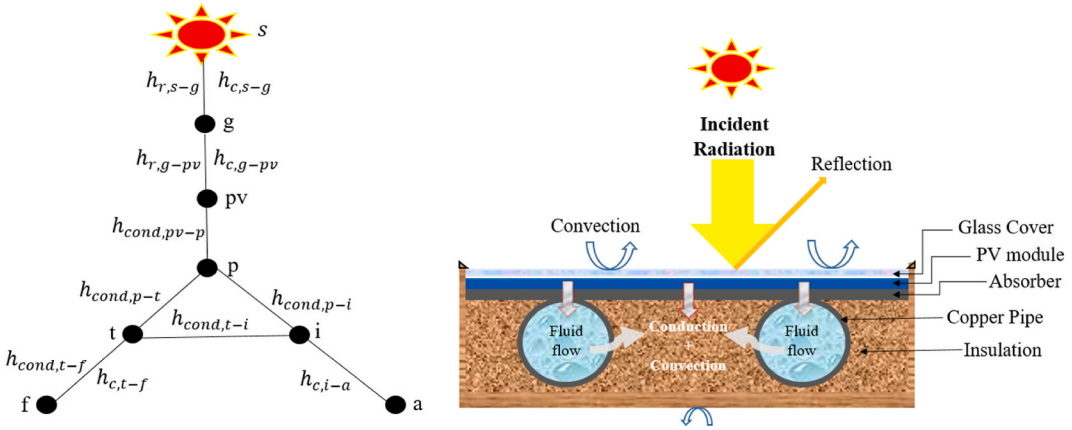

Fig. 2. Sectional view of the PV/T hybrid system and heat transfer mechanisms.

heat to be recovered by the fluid. Given the complexity of taking into account all these associated phenomena, hypotheses are put forward such as.

- ➢ The PV module and the absorber are connected in direct surface contact without adhesive glue so that there is no air space between the two components;
- ➢ Temperatures are uniform along each layer of the PV/T system and the thermophysical properties of the different materials are constant;
- ➢ The flow of fluid in the tubes is uniform and takes place along a single axis (x);
- ➢ The sky is considered a black body with a temperature T_s.

Thus, using its hypotheses and the various laws of thermodynamics, the following model is governed by mathematical equations presented below.

4.1. Energy analysis

The energy analysis carried out in this context is based on the use of the first law of thermodynamics applied to each stage/level of the PV/T system considered as shown in Fig. 2, in order to obtain an overall energy balance. The different stages/levels are the glass layer, the PV cells, the absorber plate, the tubes, the heat transfer fluid and the insulator which are represented by the indices g, pv, p, t, f and i respectively. These energy balances are evaluated by considering the path in Fig. 3. The different heat transfer modes and processes are described in Fig. 2.

Fig. 3. Process of evaluating the energy balance in the system.

4.1.1. Energy balance of the glass layer

By following this procedure in Fig. 3, the energy balance in expanded form, applied to the glass layer is given by **Eq. (1).** The glass envelope receives a flow of solar irradiation on its surface where heat exchange occurs by convection with the environment and with the ambient air below the glass. The heat flux absorbed by this layer is translated by the second term. The radiative flux passing through the glass layer goes towards the PV cells. This is materialized by the last two terms of **Eq. (1)**.

$$\boldsymbol{\rho_g \delta_g C_g \frac{dT_g}{dt} = \alpha_g G + \left(h_{c,g-pv} + h_{r,g-pv}\right)\left(T_{pv} - T_g\right) - \left(h_{r,s-g} + h_{c,s-g}\right)\left(T_g - T_a\right)} \tag{1}$$

Where $\boldsymbol{h_{c,g-pv} + h_{r,g-pv}}$ and $\boldsymbol{h_{r,s-g} + h_{c,s-g}}$ are respectively the radiative and convective heat transfer coefficients between the glass cover and the PV module for the first sum and between the glass cover and the environment for the second sum which, respectively, are given by the expressions Eq. **(2), Eq. (3), Eq. (4) and Eq. (5)** [4,32]**:**

$$\boldsymbol{h_{c,g-pv} = \frac{N_u \lambda_a}{\delta_a}} \tag{2}$$

$$h_{(r,g-pv)} = \frac{\sigma\left(T_g^2 + T_{pv}^2\right)\left(T_g - T_{pv}\right)}{\frac{1}{\varepsilon_g} + \frac{1}{\varepsilon_{pv}} - 1} \tag{3}$$

$$\boldsymbol{h_{(r,s-g)} = \frac{\sigma \varepsilon_g \left(T_g^4 - T_s^4\right)}{\left(T_a - T_g\right)}} \tag{4}$$

$$\begin{cases} h_{(c,s\text{-}g)} = 3.8V + 5.7 \\ h_{(c,s\text{-}g)} = V^{0.78} + 6.47 \end{cases} \text{Respectively for V } < 5 \textit{ and } V > 5 \frac{\text{m}}{\text{s}}. \tag{5}$$

The relationship of Hollands et al. [41] between the Nusselt number and the Rayleigh number for angles from 0° to 75° allows us to write the relationship given by **Eq. (6)**:

$$N_u = 1 + 1.44\left[1 - \frac{1708}{Ra\cos(\beta)}\right]^+ \left[1 - \frac{1708[\sin(1.8\beta)]^{1.6}}{Ra\cos(\beta)}\right] + \left[\left(\frac{Ra\cos(\beta)}{5830}\right)^{\frac{1}{3}} - 1\right]^+ \tag{6}$$

The superscript + means that only positive values of terms in square brackets should be defined (i.e. use zero if the term is negative). Ra is the Rayleigh number expressed by **Eq. (7).**

$$Ra = \frac{g.\beta'.\delta_a^3}{k_a \mu_a}\left(T_{pv} - T_g\right) \tag{7}$$

4.1.2. Energy balance on PV cells

In the case of PV cells, the energy balance follows the same path as that applied to the glass roof. Thus, the relationship obtained is given by **Eq. (8).** It takes into account the heat flow entering the PV cells which is translated into the second term multiplying the absorption coefficient $\boldsymbol{\alpha_{pv}}$ of the module to the transmittance $\boldsymbol{\tau_g}$ of the glass. The third term is the convective and radiative heat exchange between the glass cover and the PV cells. Then the fourth term characterizes the exchange by conduction between the PV cells and the absorber plate. The fifth term is the electrical energy produced. There is no exchange of energy with the outside world in this layer.

$$\boldsymbol{\rho_{pv} \delta_{pv} C_{pv} \frac{dT_{pv}}{dt} = \alpha_{pv} \tau_g G + \left(h_{c,g-pv} + h_{r,g-pv}\right)\left(T_g - T_{pv}\right) + h_{cond,pv-p}\left(T_p - T_{pv}\right) - E_{elec}} \tag{8}$$

With $h_{cond,pv-p}$ the conduction transfer coefficient between the PV module and the absorber can be calculated from Eq. (9) [4].

$$\boldsymbol{h_{cond,pv-p} = \frac{1}{\left(\frac{\delta_{pv}}{K_{pv}} + \frac{\delta_p}{K_p}\right)}} \tag{9}$$

4.1.3. Energy balance on the absorbent plate

The absorber plate is included between the PV module, the tubes and the insulation. It is a black layer material, used to absorb heat from the PV module. Its balance is given by **Eq. (10).** This layer is only dominated by transfer by conduction, because not being directly exposed to sunlight, there is no direct heat input with the sun, nor exchange by convection due to the surface close contact.

$$\boldsymbol{\rho_p \delta_p C_p \frac{dT_p}{dt} = h_{cond,pv-p}\left(T_p - T_{pv}\right) + h_{cond,p-t}\left(T_t - T_p\right) + h_{cond,p-i}\left(T_i - T_p\right)} \tag{10}$$

With $\boldsymbol{h_{cond,p-t}}$ and $\boldsymbol{h_{cond,p-i}}$ the transfer coefficients by conduction between the absorber and the tubes then between the absorber and the insulator are respectively given by the relations Eq. (11) and Eq. (12) [4,31].

$$h_{cond,p-t} = \frac{8\delta_p L K_p}{A(W - D_o)} \tag{11}$$

$$h_{cond,p-i} = \frac{2K_i}{\delta_i}\left(\frac{W - D_o}{W}\right) \tag{12}$$

4.1.4. Energy balance at tube level

The circulation of the fluid in the tubes leads to two types of heat transfer, in particular by conduction between the absorber and the tubes and also between the tubes and the insulator, then by convection between the tubes and the fluid. The energy balance at this level is expressed in **Eq. (13)**.

$$m_t C_t \frac{dT_t}{dt} = A_{pt} h_{cond,p-t}(T_t - T_p) + A_{tf} h_{c,t-f}(T_f - T_t) + A_{ti} h_{cond,t-i}(T_i - T_t) \tag{13}$$

Terms $h_{cond,t-i}$ **And** $h_{c,t-f}$ respectively designate the heat transfer coefficients by conduction between the tubes and the insulation then by convection between the tubes and the fluids circulating inside expressed by **Eq. (14)** and **Eq. (15)**. The expressions $A_{tf} = \pi D_{in} L$ **and** $A_{ti} = \left(\frac{\pi}{2}+1\right) D_o L$ represent respectively the contact surface between the tubes and the fluids then between the tubes and the insulator [32,42].

$$h_{cond,t-i} = \frac{2K_i}{\delta_i} \tag{14}$$

$$h_{c,t-f} = \frac{N_u K_f}{D_i} \tag{15}$$

4.1.5. Energy balance at the heat transfer fluid level

Following the process in Fig. 3, the expression of the energy balance at the level of the heat transfer fluid is expressed by **Eq. (16)**. The first term in the equation is the amount of energy stored in the heat transfer fluid. The second term expresses the quantity of heat transferred to the fluid by the tubes. The third term reflects the quantity of heat transferred to the heat transfer fluid by the supply of a mass of heat transfer fluid at a given temperature at the inlet of the collector and by the extraction of the same mass of heat transfer fluid at a different temperature at the one at the exit.

$$m_f C_f \frac{dT_f}{dt} = A_{tf} h_{c,t-f}(T_t - T_f) + \dot{m}_f C_f (T_{fo} - T_{fi}) \tag{16}$$

Or T_{fo} And T_{fi} are the temperatures of the fluid at the outlet and at the inlet [32].

4.1.6. Energy balance on the insulation

The insulation below the PV/T collector is in contact with the tubes and part of the absorber then with the ambient air. Its energy balance can therefore be expressed by **Eq. (17)**. This is dominated by heat exchanges by conduction between the tubes and the absorber and by convection with the ambient air.

$$m_i C_i \frac{dT_i}{dt} = A_{ti} h_{cond,t-i}(T_t - T_i) + A_{pi} h_{cond,p-i}(T_i - T_p) - A h_{c,i-a}(T_i - T_a) \tag{17}$$

The term $h_{c,i-a}$ represents the convective transfer coefficient between the insulation and the ambient air which is identical to $h_{c,s-g}$ [42].

4.1.7. Thermal efficiency

One of the parameters for assessing the performance of an energy system is its efficiency. Thus, the relationship allowing to express that of the PV/T system in this study is expressed by Eq. (18) [31], which is a function of the mass flow rate of the fluid expressed in kg/m^2, its specific heat capacity expressed in J/kg.K and the solar radiation expressed in Wh/m^2.

$$\eta_{en} = \frac{\dot{m}_f C_f (T_{fo} - T_{fi})}{GA} \tag{18}$$

4.2. Exergy analysis

The exergy analysis in this study makes it possible to assess the quality of the energy provided by the PV/T system. The details of the exergy balance are specified in Ref. [43]**.** The electrical exergy efficiency which is the ratio of the useful electrical exergy to the exergy of solar radiation is estimated at ' **Eq. (**19) [6]**.** More in-depth details of the calculation of pressure losses and friction are detailed in Refs. [31,32,42,44].

$$\eta_{ex,el}=\frac{GA_c\eta_o[1-\beta(T_c-T_a)]-\frac{m_f\times\Delta_p}{\rho_f\times\eta_{pump}}}{GA\left[1-\frac{4}{3}\left(\frac{T_a}{T_s}\right)+\frac{1}{3}\left(\frac{T_a}{T_s}\right)^4\right]} \tag{19}$$

The thermal exergy efficiency can be obtained from Eq. **(20)** [2].

$$\eta_{ex,th}=\frac{m_f\times C_f\left[T_{fo}-T_{fi}-ln\left(\frac{T_{fo}}{T_{fi}}\right)\right]}{GA\left[1-\frac{4}{3}\left(\frac{T_a}{T_s}\right)+\frac{1}{3}\left(\frac{T_a}{T_s}\right)^4\right]} \tag{20}$$

T_s is the temperature of the sun which is a function of the ambient temperature given by Eq. (21) [45]:

$$T_s=0.0552T_a^{1.5} \tag{21}$$

The mixing processes and governing equations of its models are given in Table 2. The thermophysical and rheological properties of Therminol 66, Therminol VP-1, Treated water and Untreated water come from Refs [45], while those of Palm, Cotton come from Refs. [25,46].

5. Environmental and economic models

Economic and environmental aspects in the evaluation of performance and use of energy systems are necessary in the final decision making of decision makers. The solar PV/T system proposed in this study will be evaluated in addition to the technical but economic and environmental point of view through a few indicators or parameters selected from the literature.

5.1. Environmental analysis

5.1.1. Emission rate (TE)

It makes it possible to evaluate the quantity of gas CO_2 emitted by the system during its life cycle. It can therefore be estimated using **Eq. (22)** in which *e* is the emission factor of CO_2 a value of 0.04 kg/kWh [47]:

$$\mathrm{TE}=\mathrm{e}\times\sum_{month=1}^{12}\left((E_{el}\times 0.38)+E_{th}\right)_{month} \tag{22}$$

5.1.2. Cost of energy (COE)

The levelized cost of energy can be evaluated through **Eq. (23)** [47]. It specifies the unit price at which the energy produced will be marketed.

$$COE=\frac{TAC}{\sum_{month=1}^{12}\left((E_{el}\times 0.38)+E_{th}\right)_{month}} \tag{23}$$

The term TAC represents the total annual cost which is given by **Eq. (24)** [17], in which CRF represents the capital recovery factor estimated by **Eq. (25)** [48]. It is a factor that determines how long the savings offset the upfront costs.

$$TAC=CRFC_i\left(1+\frac{C_o}{C_i}-\frac{SV}{C_i}\right) \tag{24}$$

$$CRF=\frac{i_i(1+i_i)^n}{(1+i_i)^n-1} \tag{25}$$

With *i* which represents the inplateletsion rate and *n* the number of years of life of the system set at 23 years. The term C_i represents the initial investment cost given by **Eq. (26)**. It takes into account the unit price of each component of the system [43].

$$C_i=1.5\left[a_1\left(A_p\right)^{b_1}+a_2(A_t)^{b_2}+a_3(V_i)^{b_3}+a_4\left(A_g\right)^{b_4}+a_5(A_c)^{b_5}\right]+a_6\left(\dot{W}_p\right)^{b_6}+\left(a_7+C_{bf}\right)L_t n_t\varphi\rho_{nf}\left(\frac{\pi d_i^2}{4}\right) \tag{26}$$

The coefficients a_i in b_i the relation Eq (25) represent the unit prices of the components of the hybrid PV/T system respectively [120 60,220 4.5400 3500 40], [0.9 0.8 1 1 1.01 0.47]. The term C_{bf} is the unit price of the base fluid. C_o is the operational and maintenance cost estimated from **Eq. (27)**, in which C_{el} is the average unit price of a kWh of electricity which is 0.33 $/kWh [3], t_y is the annual operating time.

$$C_o=C_{el}t_y\dot{W}_p \tag{27}$$

Untreated water is considered to be water coming from the sea, rivers or rivers. On the other hand, treated water is that which has

undergone treatments with the aim of making it healthier and generally for human consumption. For synthetic oils (TH66 and THVP1), these prices take into account export costs. The different unit prices are presented in Table 3.

The recovery value (SV), which is simply the gain generated by the system at its end of life, can be estimated from **Eq. (28)** [30]. It therefore reflects the value that the system can have by reselling it at the end of its life.

$$SV = \frac{0.23 C_i}{(1+i_i)^n} \tag{28}$$

5.2. Economic analysis

5.2.1. Net present value (NPV)

It is the financial indicator that assesses the viability of the investment. It takes into account the future cash flow on the initial investment. A positive NPV is advantageous for the profitability of a project. Its expression is given by **Eq. (29)** [30], in which LCC represents the set of savings achieved during the life cycle which takes into account all the costs and benefits associated with the production of energy during its life cycle. Its expression is given by Eq. (30) [24,29].

$$NPV = \left(\frac{LCC}{i_d - i_i}\right)\left[1 - \left(\frac{1+i_i}{1+i_d}\right)^n\right] - C_i \tag{29}$$

$$LCC = \frac{(1+i_i)^{n-1}}{(1+i_d)^n}\left[C_{el}\sum_{month=1}^{12}(E_{el})_{month} + C_{th}\sum_{month=1}^{12}(E_{th})_{month}\right] \tag{30}$$

The coefficient C_{th} represents the average cost of thermal energy (0.54 $ USD/kWh) [3].

5.2.1.1. Time to return on investment (CPBT). This is the amount of time it will take to recover the total investment cost. It is given by the expression **Eq. (31)** [32].

$$CPBT = \frac{C_i}{C_{el} \times ((E_{el} \times 0.38) + E_{th})} \tag{31}$$

5.2.2. Exergy sustainability index

One of the objective functions is the exergy sustainability index. It assesses the net energy efficiency and environmental sustainability of a system. It is calculated by **Eq. (32)**:

$$SI = \frac{1}{1 - \eta_{ex,overall}} \tag{32}$$

6. Digital model

The equations of the different balances being coupled, a numerical resolution of these equations is appropriate. The Gauss-Seidel method, which is an iterative method using values calculated in the previous iteration to obtain new values, is implemented in the Matlab software. The choice of the Gauss-Siedel method is therefore important for this case, thanks to its rapid convergence and its precision.

The equations governing the different energy balances are first discretized using finite differences to have a linear form. It consists of replacing continuous variables with sampling points defined in time as presented in **Eq. (33)**. The flowchart in Fig. 5 presents the numerical simulation procedure as well as the boundary conditions. The input data are presented in Table 4.

$$\frac{\boldsymbol{dT_{layer}}}{\boldsymbol{dt}} = \frac{\boldsymbol{T_{layer}^{t+\Delta t}} - \boldsymbol{T_{layer}^{t}}}{\boldsymbol{\Delta t}} \tag{33}$$

Where n and Δt represents the time index and the discrete step respectively. The different balances are put in matrix form (AT = B), where A is a square matrix and B is the column vector containing the source terms of each discrete equation. The different wall temperatures are determined as shown in the flowchart in Fig. 4. For accuracy beyond high calculation time, the process is performed

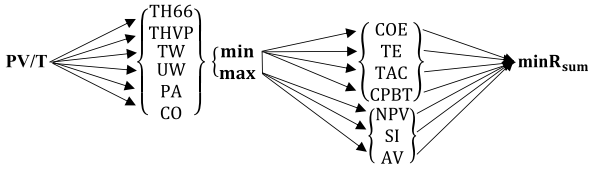

Fig. 4. Formulation of the optimization problem.

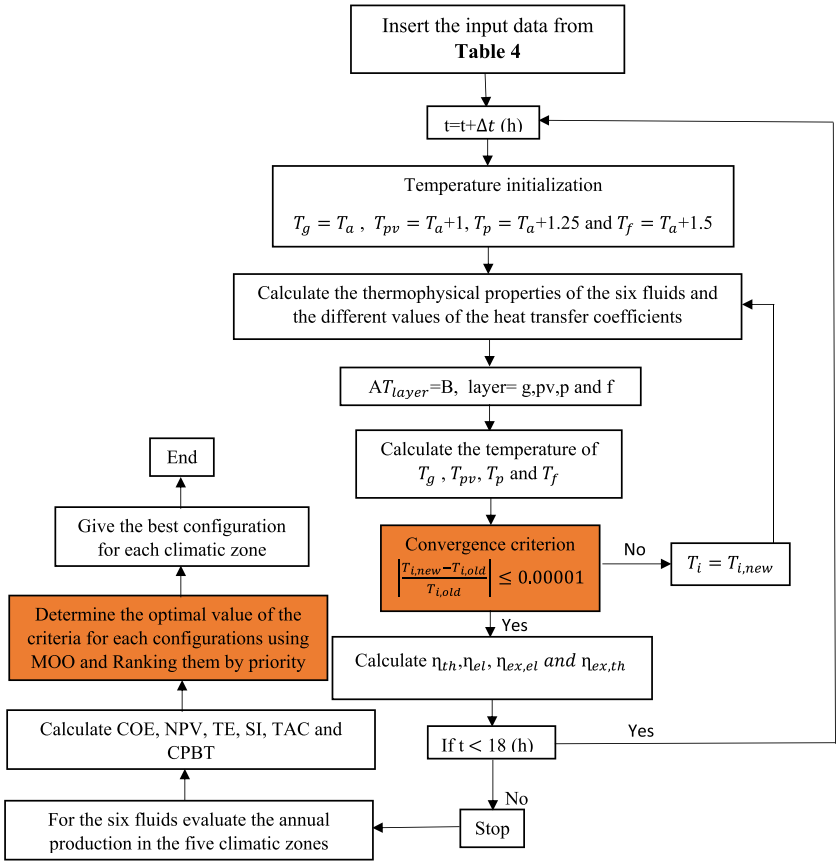

Fig. 5. Calculation flowchart.

for every deviation less than 10^{-5} until the test end time. After that, the different efficiencies are evaluated and economic parameters are calculated for decision making.

6.1. Formulation of the optimization problem

The technique used here is multi-objective optimization (MOO) to search for optimal solutions. Thus, the selection of the best system will be based on four objective functions to minimize (COE, TE, TAC and CPBT) and three objective functions to maximize (NPV, SI and AV) whose diagram is given by Eq. **(34)**. These functions are key points of the 4E analysis. The AV criterion is the availability parameter which takes into account local production, proximity and quantity of fluid in the area. Because the operation of the solar system must be continuous and thus the fluid must be constantly available and in large quantities. Each system is therefore classified according to its rank and the best system is the one whose rank is closest to 1. For systems having a total rank (R_{sum}) identical, priority will be given to the system with a lowest COE, that This is to relieve the population, the majority of whom are very poor.

$$R_{sum} = R_{COE} + R_{NPV} + R_{TE} + R_{TAC} + R_{CPBT} + R_{SI} + R_{AV} \tag{34}$$

6.2. Statistical indicator

For model validation, the relative error (RE) given by Eq. (35) is used to evaluate the performance of the proposed system [36]. It makes it possible to measure the gap between this model and the different models present in the literature.

$$RE = \frac{1}{n}\sum_{i=1}^{n}\left(\frac{|Sim - Exp|}{Exp}\right) \tag{35}$$

7. Results and discussions

The instantaneous and daily evaluation of the system parameters is carried out using the Capderou solar radiation estimation model [49]. It is used for its simplicity which is based on mathematical equations based on the elevation angle of the sun at different times of

the day. The thermal behavior of the different thermophysical properties of the nanofluids following temperature variation, used in this study is presented in Fig. 6.

The different configurations of HTFs used in this study behave differently following temperature variation. These thermal behaviors can be observed in Fig. 6 through thermophysical properties such as density (Fig. 6a), specific heat (Fig. 6b), thermal conductivity (Fig. 6c) and dynamic vicosity (Fig. 6d) of fluids. For a variation from 20 to 80 °C in steps of 10 °C, the density (Fig. 6a) and dynamic viscosity (Fig. 6d) of all configurations of HTFs based on TiO_2 (4 %) are more sensitive to the increase in temperature. While their thermal conductivity (Fig. 6c) and thermal capacity (Fig. 6b) are less sensitive to temperature. It is also notable that increased temperature of NFS lowers the viscosity and slightly the conductivity of the oils. On the other hand, it has a good effect on both types of water. May be due to the different chemical composition of each. This provides information on their possible influence on the performance of the PV/T system.

In **sections 7.1 and 7.2**, the city of Yaoundé and the month of March are considered because of its climatic specificities according to Ref. [16], and according to the day recommended by Klein [49].

7.1. Validation of the numerical model

To assess the PV/T system model proposed in this study, different validations were carried out at different levels in terms of thermal and electrical performance. The results of output parameters such as cell temperature, thermal and electrical efficiency of the system are compared to those obtained numerically and experimentally in the literature.

7.1.1. Validation of PV cell temperature

For solar radiation of 1000 W/m^2 and an input flow rate of 0.025 kg/s, the output temperature of the PV cells of the present work and that of Ref. [27] are compared in Table 5. The relative error between the two models is 2.4 %. This difference, considered quite

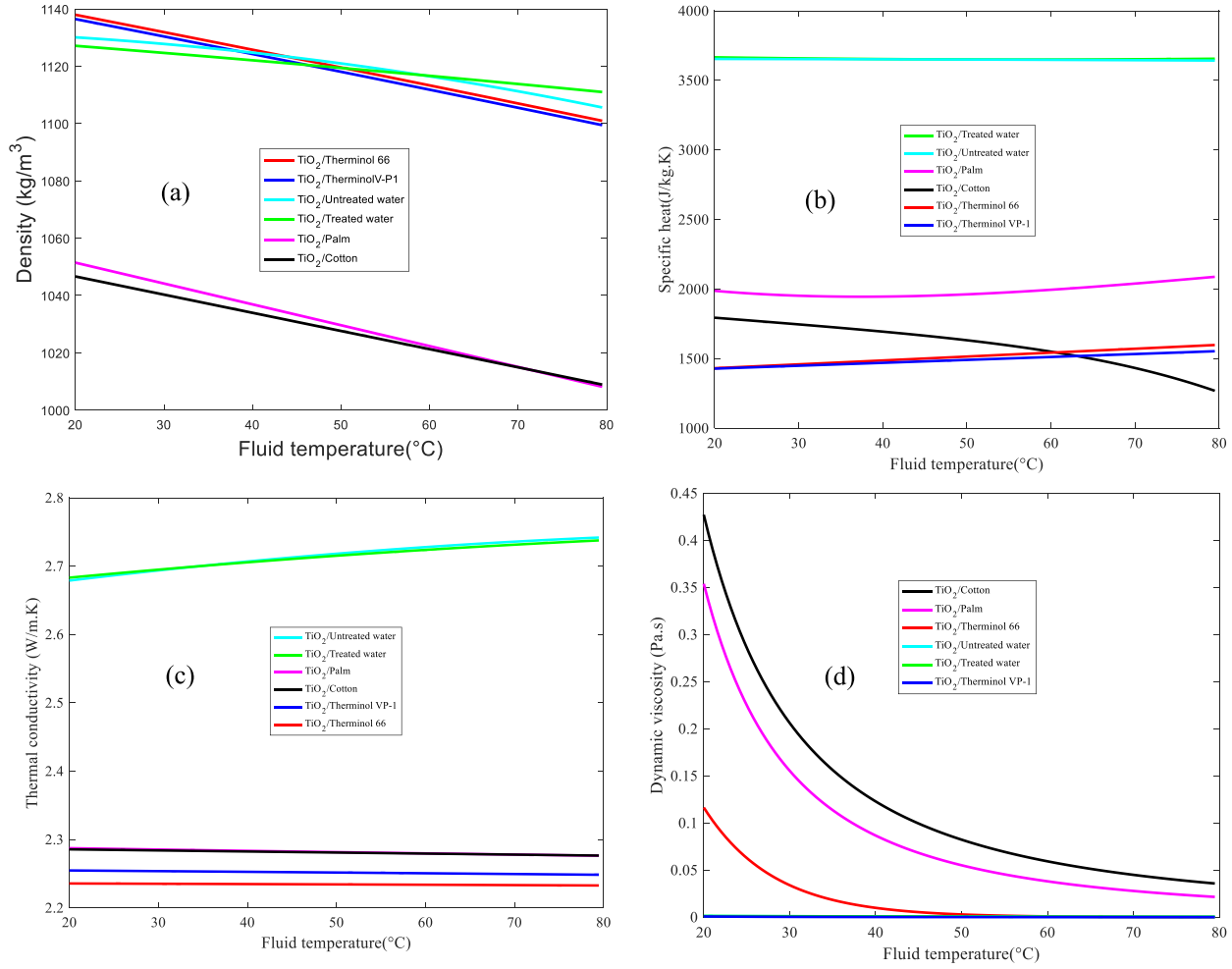

Fig. 6. Sensitivity to temperature variations of density (a), specific heat (b), thermal conductivity (c) and dynamic vicosity (d) of fluids.

Table 5
Validation of the current model through the temperature of the PV cells.

	Solar radiation (W/m^2)	Flow rate (kg/s)	T_{PV} (°C)
Present work PV/T-PA/ TiO_2	1000	0.025	52.8
PV/T-PA/Ti_3C_2 [27]	1000	0.025	54.10
Error (%)			2.4

good, can be attributed to the differentiated effects of the configuration of the fluids used.

7.1.2. Validation of the thermal and electrical yields of the PV/T system

The thermal and electrical efficiencies of the PV/T-UW solar system are used to validate the results of the current model by comparing them to the experimental values of Ref. [50] in Table 6. The values of ambient temperature and solar irradiation related to the experiment are used as input parameters in this simulation. Seven (7) tests were carried out, on average the absolute deviation obtained is 2.68 % considering the thermal efficiency and 2.88 % considering the electrical efficiency.

The maximum relative difference observed between different measured and predicted values of thermal and electrical efficiencies is not greater than 3 %, as is the relative error.

These slight errors can be justified by the thermo-physical properties of the components of the hybrid PV/T sensor taken as constants during these simulations. This verifies the accuracy of this numerical model which could be used for future research.

7.2. Evaluation of energy and exergy performances

Evaluation of the transfer coefficient by convection as a function of the morphology and volume concentration of the NPs.

Seven (7) geometric shapes of the nanoparticles are considered in this study. Blade, brick, cylindrical, platelets, spherical, film and wire shapes are taken into account in this study. The first four being directly linked to the dynamic viscosity and the others to the specific capacity which is dependent on the diameter of the NPs. The variation of the convective heat transfer coefficient between the CO/NFs TiO_2 and the tubes as a function of the morphology and the volume concentration of the nanoparticles is shown in Fig. 7. Solar irradiation and ambient temperature are set at 800 W/m^2 and 25 °C respectively. The nanofluid based on the treated water is the HTF configuration used with a mass flow rate of 0.087 kg/s.

The convection transfer coefficient increases with the volume concentration. This result was found by Ref. [46] using Ti_3C_2/TW. However, above 4.4 % the increase is more significant than below 4.4 % which is less significant. This can be attributed to the specific thermal effects of TiO_2 in the untreated water base fluid. In terms of NP morphology, the shapes evaluated in Fig. 7 a are more sensitive than that of Fig. 7 b. NPs having the shape of lamellae or spheres increase the transfer coefficient by convection between the fluid and the tubes. On the other hand, NPs approaching the platelets form have the smallest transfer coefficient by convection with increased concentration. This could be due to the size of each NP which, when very high, increases the contact surface with the fluid as well as the heat transfer.

7.2.1. Hourly evaluation of PV/T collector temperatures

Fig. 8 presents the hourly evolution of the temperatures of the PV cells, the outlet fluid and the glass cover for each of the HTFs configurations. NPs in the form of lamellae and spheres are used. The PV/T configurations shown are with TH66/TiO2 (Fig. 8a), THVP1/TiO2 (Fig. 8b), TW/TiO2 (Fig. 8c), UW/TiO2 (Fig. 8d), PA/TiO2 (Fig. 8e) and CO/TiO2 (Fig. 8f). The temperature of thermal oils increases more quickly reaching high values than that of vegetable oils, which was found and justified by Ref. [26] in the case of parabolic trough solar collectors. The PV/T-CO/TiO_2 system maintains the temperature of the PV cells below 36 °C, with an outlet temperature of 35.6 °C. It can also be observed that PV/T-PA/TiO_2 maintains the cell surface at a temperature below 43 °C throughout the day. This was also verified by Ref. [27] who achieved a maximum cell temperature of 42.5 °C with Mxene/palm at 0.07 kg/s.

PV/T-TW/TiO_2 systems and PV/T-UW/TiO_2 present the greatest differences between the temperatures of the cells and the leaving water. The PV/T-TH66/TiO_2 and PV/T-THVP1/TiO_2 system have the highest output temperatures which are very close to the

Table 6
Validation of electrical and thermal efficiency with data from Ref [50].

Test	Ta (°C)	H (MJ/m^2)	$\eta_{th,Exp}$ (%) [50]	$\eta_{th,Sim}$ (%) Present work	Error	$\eta_{e,Exp}$ (%) [50]	$\eta_{e,Sim}$ (%) Present work	Error
1	36.7	16.14	41.34	41.39	0.12	9.84	10.01	1.72
2	35.9	14.57	43.20	42.60	1.38	10.49	10.43	0.57
3	33.0	12.94	38.85	40.22	3.52	9.01	10.15	12.65
4	29.6	16.87	41.07	39.35	4.18	11.27	11.29	0.17
5	22.0	11.66	38.34	38.33	0.02	11.39	11.41	0.17
6	19.39	13.82	43.51	42.89	1.42	12.22	12.43	1.71
7	16.1	13.61	40.27	40.17	0.24	11.93	12.30	3.1
RE(%)					**1.55**			**2.87**

RE: Relative Error.

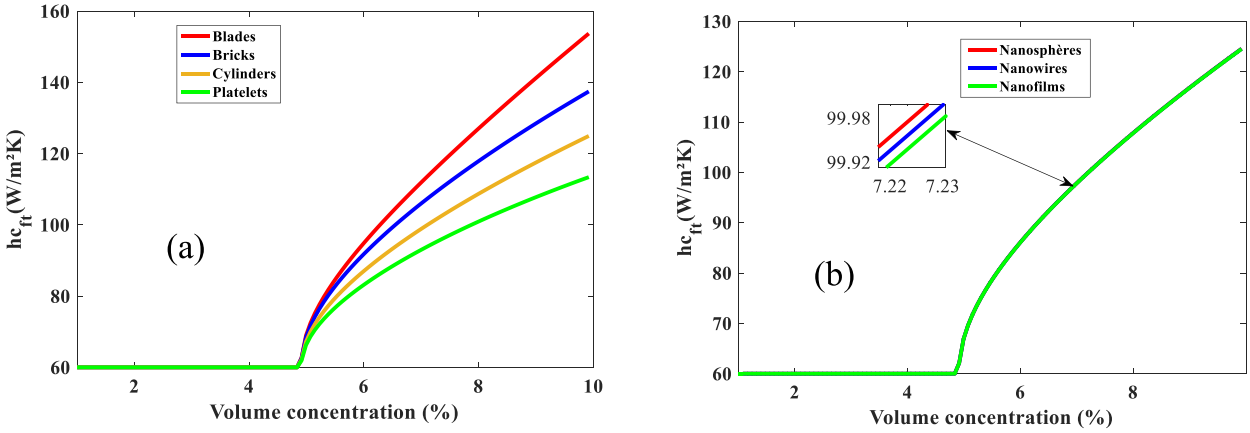

Fig. 7. Variation of the heat transfer coefficient by convection between the fluid and the tubes taking into account type 1 (a) and type 2 (b) of morphology as a function of the volume concentration of the nanoparticles.

temperature of the PV cells. We could say that the temperature of the Therminol increases approximately equally with that of the PV module but they do not cool the latter enough. This effect could be due to the direct PV-absorber-tubes contact and also to their low thermal capacity.

Fig. 9 shows the instantaneous temperature of PV cells of the PV/T system with different HTF configurations. Cottonseed oil, due to its very high viscosity and low thermal conductivity, has better performance in terms of cooling, followed by treated water, palm oil, untreated water, Therminol 66 and VP-1 with a maximum cell temperature of 35 °C, 41 °C, 42.8 °C, 46.1 °C, 51.3 °C and 54.07 °C respectively around 12 h.

7.2.2. Influence of the mass flow on the outlet temperature of the different configurations of the HTFs

Fig. 10 presents the influence of the mass flow on the outlet temperature of the HTFs configurations. Notably for the PV/T configurations of TH66 (Fig. 10a), THVP1 (Fig. 10b), TW (c), UW (Fig. 10d), PA (Fig. 10e) and CO (Fig. 10f) with and without TiO_2 as a function of mass flow. This influence is analyzed by comparing two configurations of the same basic HTF (with nanoparticle and without nanoparticle). The volume fraction is set at 4 % according to the analysis made in Fig. 7 and the inlet temperature of the HTFs is taken equal to 30 °C. It can be observed that the outlet temperature of the HTFs decreases with the increase in mass flow and then stabilizes at a certain value. This can be justified by the fact that a very high flow rate does not help the HTF to store heat well due to its reduced contact time with the tubes. However, more or less significant differences between the systems operating with NF and the base fluids are observed. On average across all configurations, the impact of nanoparticles is significant when comparing the exit temperature of the nanofluids to the base fluids under different mass flow rates. On average, the effects are more significant with the configuration based on synthetic oils (TH66/TiO_2 and TH66 with a difference of 1.23 °C, THVP1/TiO_2 and THVP1 with a difference of 0.93 °C), based on oils plant-based (CO/TiO_2 and CO with a difference of 1.13 °C) and water-based (TW/TiO_2 and TW with a difference of 0.61 °C, UW/TiO_2 and UW with a difference of 0.60 °C) respectively.

7.2.3. Power consumed by the pump for each system

In Fig. 11, the variation of the power consumed by the pump as a function of the flow rate of each NF is presented. It is seen that the higher the flow rate, the more electricity the pump consumes. It clearly emerges that nanofluids based on vegetable oils (Fig. 11a) and particularly cotton consume nearly 23.8 mW while treated water (Fig. 11b) is around 1 mW at 0.01 kg/s. This is attributed to the viscosity of the oils which increases with the addition of NPs. For the case of Fig. 12 b, although the viscosity of synthetic oils are higher, the work provided by the pump is lower compared to the configuration with the water-based Nf. This observation could be due to a higher pressure loss with the Nfs UW/TiO_2 and TW/TiO_2. Can be justified by the interaction between molecules more considerable in vegetable oils than in water and even less in synthetic oils at a high flow rate. This result is confirmed by the authors of ref. [44], who proved that the increase in TNF flow rate is conditioned by the increase in pump power. Pump consumption therefore probably has an impact on energy production.

7.2.4. Evaluation of thermal efficiency

The evaluation of the thermal efficiency of the different PV/T configurations considered is presented in Fig. 12. In Fig. 12 a, the flow rate is maintained at 0.0087 kg/s, the irradiation and the temperature are kept constant at 850 W/m^2 and 30 °C respectively. An increase in thermal efficiency can be observed with increasing NP concentration up to a threshold of approximately 4–5 %, before becoming constant. Due to their high thermal capacity, PV/T systems with water as base fluid have the highest thermal performance, followed by PV/T-PA/ TiO_2, PV/T-CO/ TiO_2, PV/T-THVP1 systems/ TiO_2 and PV/T-TH66/TiO_2 respectively. Indeed, the flow speed being average, it is possible that the viscosity of vegetable oils increases the contact time with the tubes which therefore conduct heat efficiently. Low efficiency of therminolVP-1 and therminol66 oils in the PV/T system could also be explained by a high temperature of

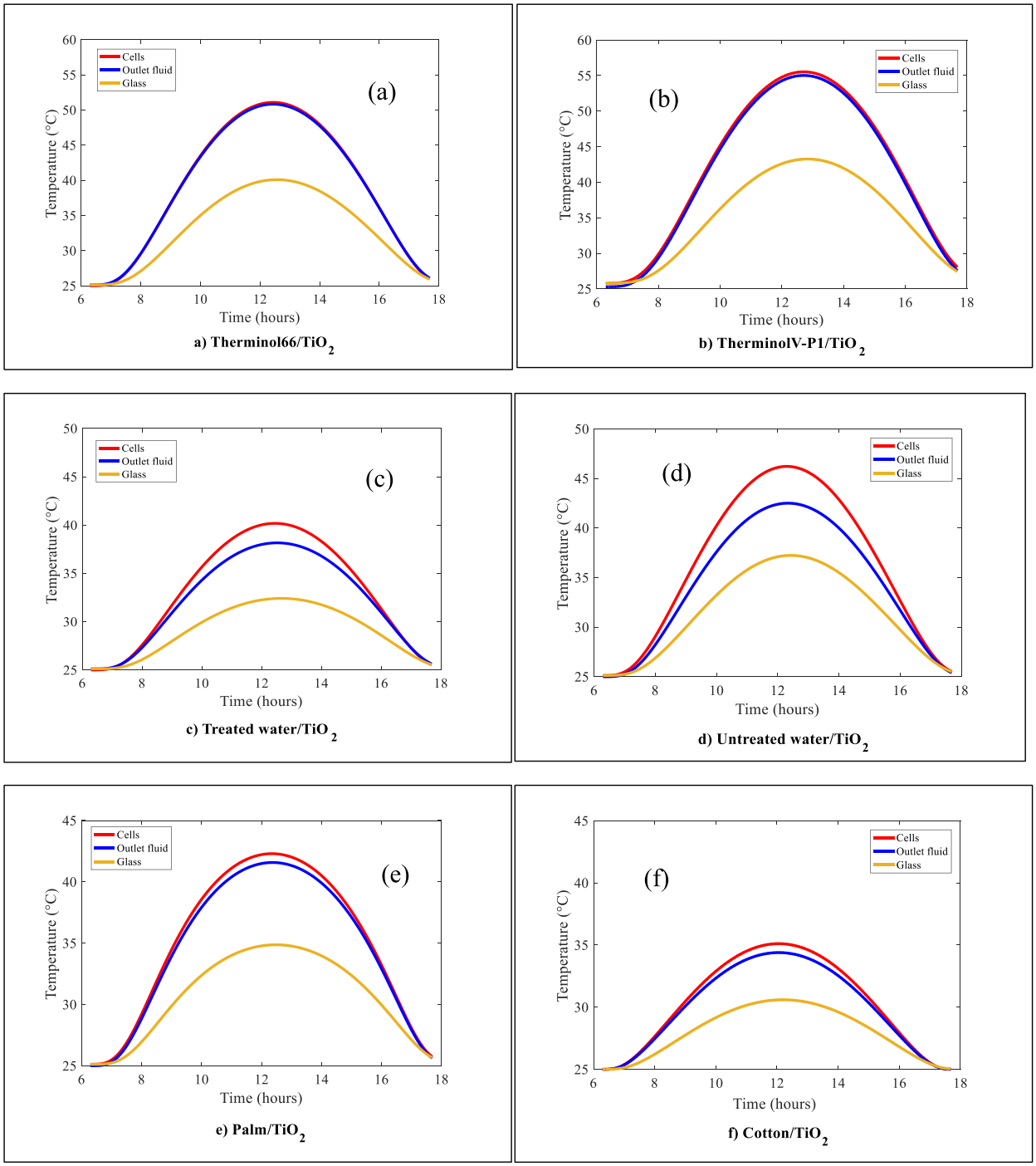

Fig. 8. Time distribution instantaneous temperatures of PV cells, outlet fluid and glass cover for different configurations of PV/T with TH66/TiO_2 (a), THVP1/TiO_2 (b), TW/TiO_2 (c), UW/TiO_2 (d), PA/TiO_2 (e) and CO/TiO_2 (f).

the glass envelope as indicated in Fig. 10 which causes enormous external heat loss at this layer. In Fig. 12 b, the effect of solar irradiation on thermal efficiency is presented and a linear growth in efficiency is observed with the increase in solar flux with differentiated effects for each configuration of HTFs on thermal efficiency. The PV/T-TW/TiO_2 and PV/T-UW/ TiO_2 systems stand out due to their higher thermal efficiencies with strong sunlight.

7.2.5. Evaluation of electrical performances

The electrical efficiency of the PV/T hybrid system mainly depends on the PV cells. So HTF with good absorption performance is

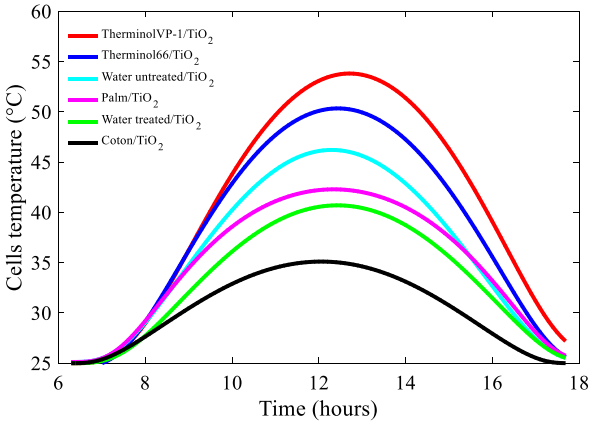

Fig. 9. Instantaneous temperatures of PV cells for different nanofluid configurations.

desirable. This can be observed in Fig. 13 which presents the instantaneous evolution of the electrical efficiency of the system with the different HTF configurations. Solar irradiation and ambient temperature are variable. We observe an improvement in electrical efficiency of 2.04 %, 3.33 %, 6.08 %, 7.5 %, 9.75 % and 12.08 % respectively with the configuration PV/T-THVP1/ TiO_2, PV/T-TH66/ TiO_2, PV/T-UW/ TiO_2, PV/T-PA/ TiO_2, PV/T-TW/ TiO_2, PV/T-CO/ TiO_2. The PV/T-CO/ TiO_2 configuration has the highest electrical efficiency due to its relatively low cell temperature during the day.

7.2.6. Energy performances produced

Fig 14 presents the electrical (Fig. 14a) and thermal (Fig. 14b) energy produced annually by each HTF configuration. Thus, the effect of seasonal variabilities is considered. It can be observed that systems with high electrical energy production have low thermal energy production. This can be explained by the fact that light conversion into electrical energy is more efficient at lower PV cell temperatures, while thermal production is higher at higher temperatures. The PV/T-CO/ TiO_2 system has the largest annual electricity production of 46.17 kWh but the smallest annual thermal energy production worth 335.7 kWh. In fact, their thermal capacity being relatively low, limits the production of thermal energy. On the other hand, the PV/T-THVP1/configuration TiO_2 produces 401.91 kWh/yr of thermal energy which is the highest with 42.10 kWh/yr of electrical energy. Which is very remarkable for applications requiring large thermal production. The configurations with the TW and UW HTFs have respectively 44.95 and 340.5, 44.61 and 361.38 kWh/yr of electricity and thermal energy produced.

Table 7 makes a comparison between the different parameters output from a few configurations chosen in this study with those from the literature. The electrical improvement is achieved by comparing the electrical performance of the uncooled PV system to the cooled PV system. A significant similarity is observed with those in the literature. In addition, the electrical improvement obtained with vegetable oils compared to those from the literature is better.

7.2.7. Exergy performance

In Fig. 15 illustrates the actual efficiency of each system. The PV/T-UW/ TiO_2 system displays the highest exergy efficiency of 25.74 % while the PV/T-THVP1/TiO_2 displays an exergy efficiency of 22.19 % which is higher than that of the PV/T-TH66/system TiO_2 with an efficiency exergy of 20.51 %, below the PV/T-TW/ TiO_2 which is at 20.47 %, then the PV/T-PA/ TiO_2 system at 18.84 % and the PV/T-CO/ TiO_2 system at 15.09 %. This illustration gives a more precise trend in the thermal and electrical performance of the PV/T system. The comparison of exergy performances with those in the literature is presented in Table 8.

7.3. Monthly assessment of energy produced in the five climate zones

Fig. 16 presents the monthly variations in global solar irradiation (Fig. 16a) and ambient temperature (Fig. 16b) during a year in five cities in Cameroon (2022). These data are available on the PVGIS website [52] which is an online software for estimating meteorological data.

In order to evaluate the annual performance of each PV/T configuration considered, the monthly electrical and thermal energy are analyzed in the different chosen cities.

Figs. 17–21 illustrate the monthly variation of electrical (a) and thermal (b) energy produced by each PV/T configuration in five climatic zones of Cameroon via the chosen cities, respectively YAOUNDE (Fig. 17a and b), MAROUA (Fig. 18a and b), NGAOUNDERE (Fig. 19a and b), DOUALA (Fig. 20a and b) and BAFOUSSAM (Fig. 21a and b). It is noted that weather conditions create significant fluctuations on the total efficiency of PV/T systems. It can be observed that the months with higher irradiation such as December, January and February have the greatest production in electrical and thermal energy. Due to the ambient temperature in Maroua, the thermal efficiency is much higher in this area whatever the configurations.

PV/T-TH66/TiO_2 and PV/T-THVP1/TiO_2 systems have better performance in very hot areas such as MAROUA, NGAOUNDERE and DOUALA. PV/T-CO/ TiO_2, PV/T-TW/ TiO_2 and PV/T-PA/ TiO_2 systems led to the highest electricity production of 125.21 kWh/yr,

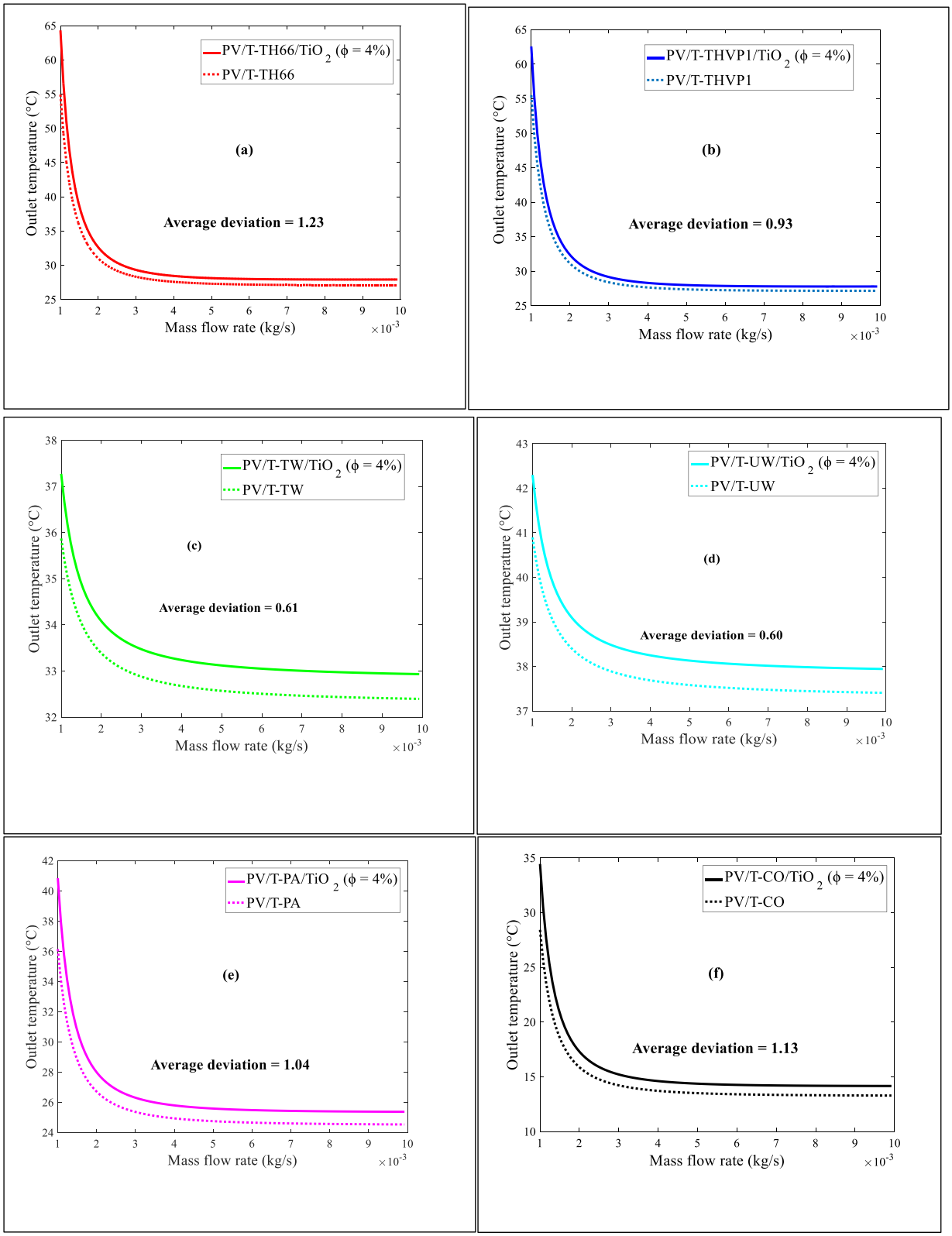

Fig. 10. Variation of fluid outlet temperature for PV/T configurations of TH66 (a), THVP1 (b), TW (c), UW (d), PA (e) and CO (f) with and without TiO_2 as a function of mass flow.

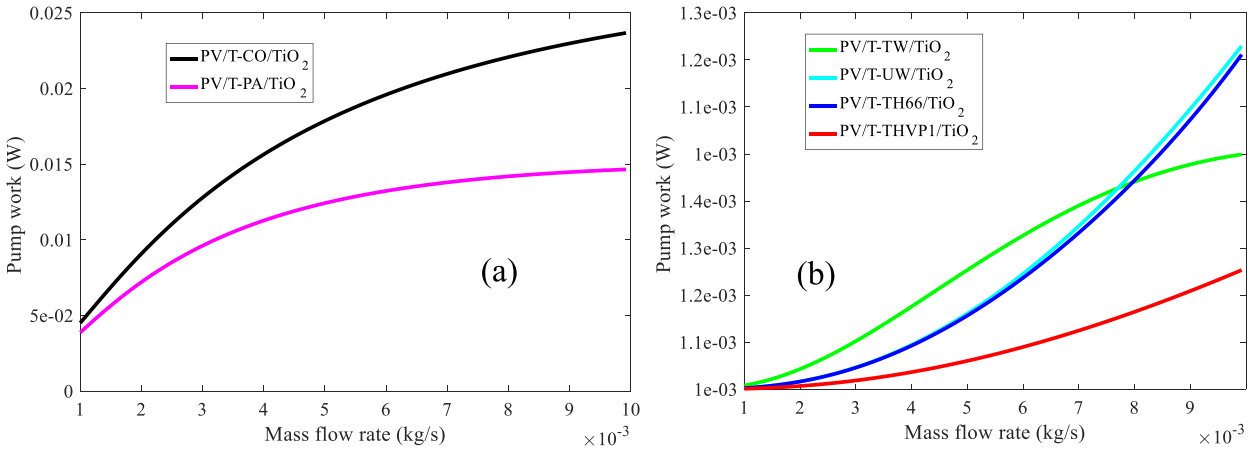

Fig. 11. Power consumed by the pump as a function of fluid flow for PV/T configurations of vegetable oils (a) and synthetic oil and water (b).

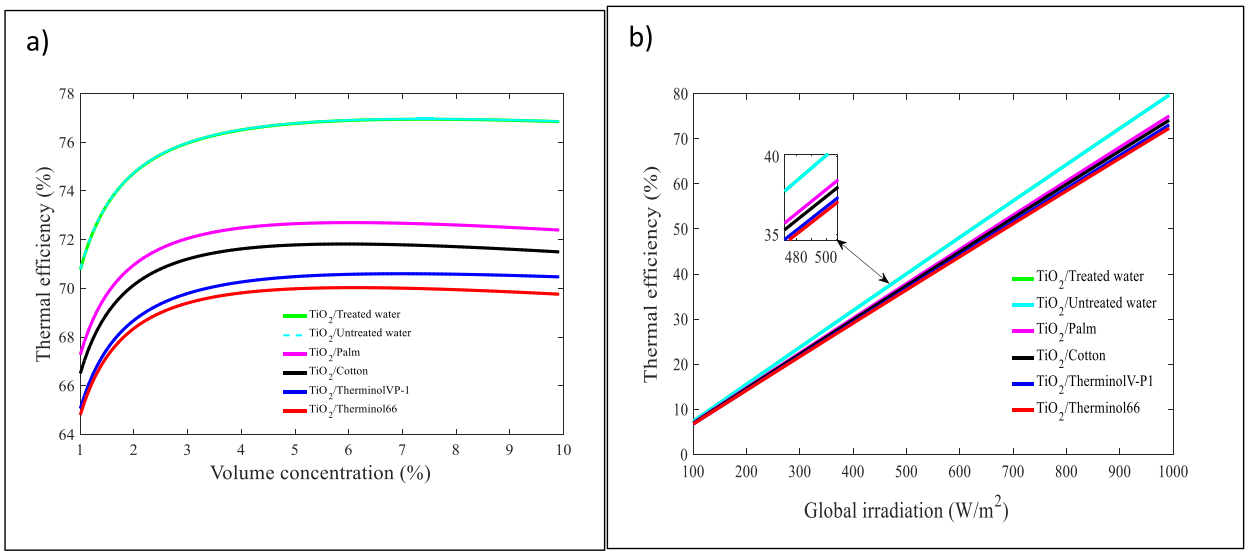

Fig. 12. Variation of thermal efficiency as a function of volume concentration (a) and solar irradiation (b).

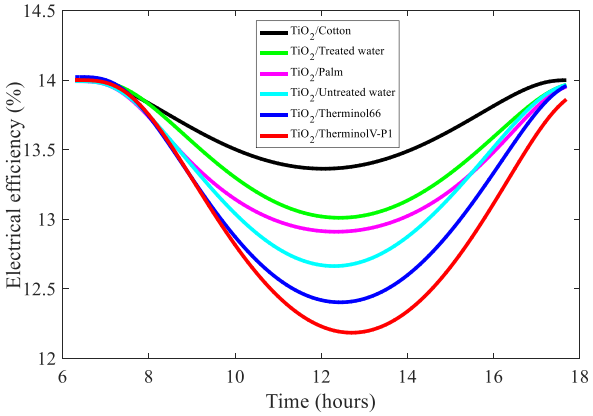

Fig. 13. Instantaneous variation of electrical efficiency.

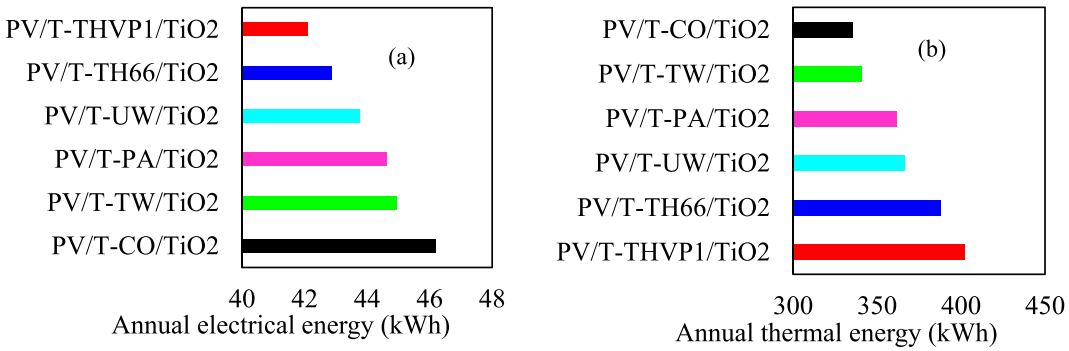

Fig. 14. Annual electrical (a) and thermal (b) energy produced for each PV/T system.

Table 7
Comparison of the energy performances of the PV/T system with those from the literature.

Study	Basefluids	Nanoparticle and concentration (%)	Global irradiation (W/ m^2)	Thermal energy produced (kWh/year)	Electric energy produced (kWh/year)	Total energy produced (kWh/yr)	Thermal efficiency (%)	Electrical efficiency (%)	Electrical improvement (%)
Present work	Palm	TiO_2	850	361.38	44.61	405.99	72.2	12.59	7.5
Present work	Cotton	TiO_2	850	335.70	46.17	381.87	71.52	13.42	12.08
Present work	Treated Water	TiO_2	850	340.50	44.95	385.45	77.12	13.09	9.75
Sohani et al. [17]	Water	TiO_2	–	–	–	626.0	45.95	14.56	5.90
Hussain and Jun-Tae [24]	Water and air	–	800–1000	–	–	197,465	52.22	14.31	14.85
Fazlay et al. [27]	Palm	Mxene (Ti_3C_2 0.125 wt%)	1000	–	–	–	79.13	13.15	15.44
Fazlay et al. [27]	Soya oil	Mxene (Ti_3C_2 0.125 wt%)	1000	–	–	–	84.25	14.20	14.3
Hussain and Jun [31]	Water	CuO	700	707	296	855	68	13.6	–
Adun et al. [44]	Water	CuO–MgO- T_iO_2 (1 %)	928	–	–	–	58.8	13.54	1.69

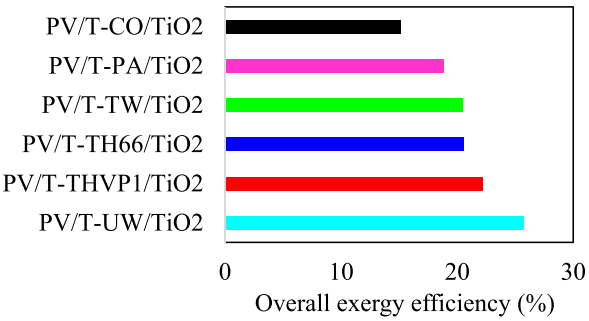

Fig. 15. Evaluation of exergy efficiency.

Table 8
Comparison of the exergy of the different configurations of the present PV/T system with those from the literature.

Study	Basefluid	G (W/ m^2)	NP and φ (%)	Overall exergetic efficiency (%)
Present work	Palm	850	TiO_2 (4 %)	18.85
Present work	Thermonol 66	850	TiO_2 (4 %)	20.51
Present work	ThermonolVP-1	850	TiO_2 (4 %)	22.19
Present work	Untreated water	850	TiO_2 (4 %)	25.74
Hussain and Jun-Tae [24]	Water and air	800–1000	–	13.85
Samir et al. [30]	C-PV/T Water	873.1	Ag (3 wt%)	13.97
Khanjari et al. [36]	water	800	Ag (5 %)	15.4
Sajid et al. [51]	PV/T-TC Water	638	–	19.03

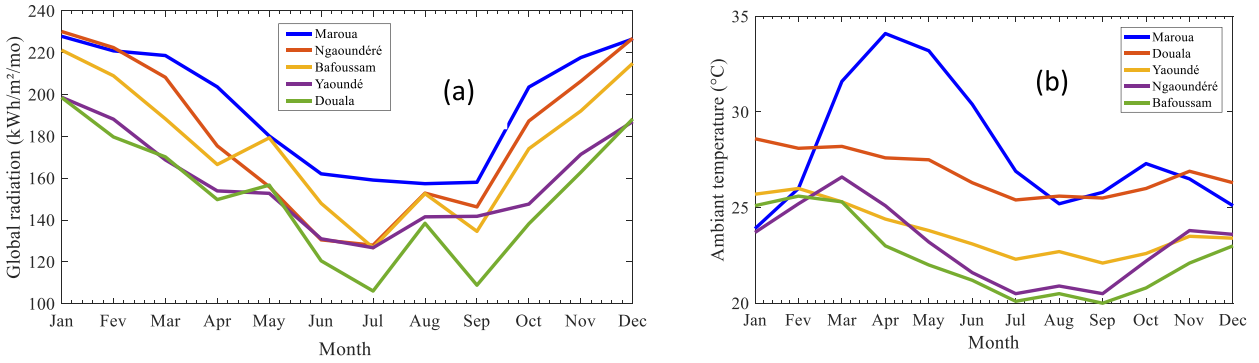

Fig. 16. Monthly variation of solar irradiation (Fig. 16a) and ambient temperature (Fig. 16b) of the different chosen cities.

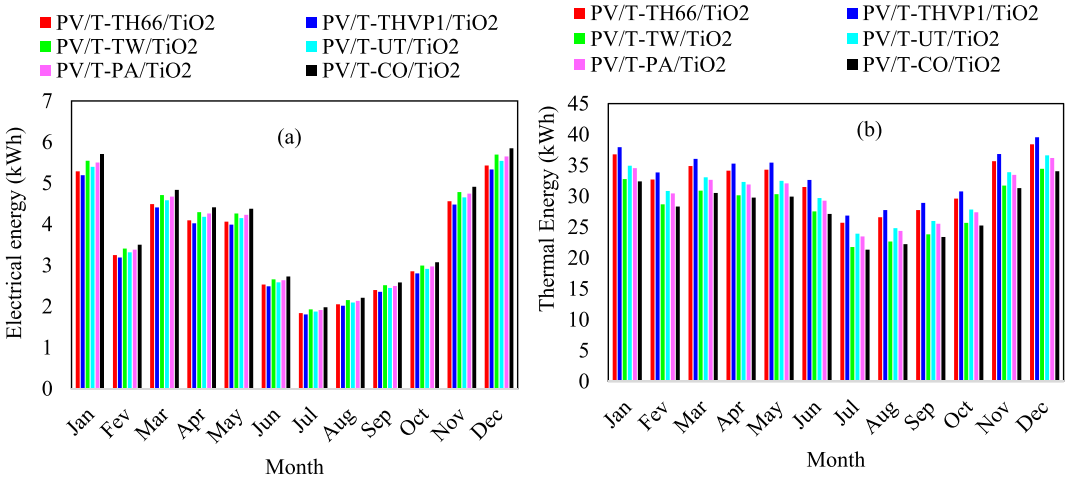

Fig. 17. Evaluation of electrical (a) and thermal (b) energy production in the YAOUNDE area.

121.91 kWh/yr and 120.97 kWh/yr respectively in the city from MAROUA. The ability of synthetic oils to store a very large quantity of heat at high temperatures therefore allows them to obtain better thermal energy production. On the other hand, in areas where the sunshine is less intense like BAFOUSSAM, vegetable oils and water have good electrical production.

7.3.1. Multi-objective analysis

Table 9 presents the different values of the decision-making parameters for each configuration and by climatic zone. Generally speaking, all the projects of the different PV/T configurations proposed in this study are viable. From an economic and environmental point of view, differences are observed between PV/T configurations.

In Yaoundé, the PV/T-THVP1/Ti O_2 configuration is economically good with a CPBT of around 5 years and 7 months but PV/T-CO/Ti O_2 has the best eco-balance of a TE of 6.9516 kg/yr. On average, PV/T-UW/Ti O_2 is the best configuration.

In Maroua, the PV/T-THVP1/Ti O_2 configuration is economically good with a CPBT of around 5 years and 11 months but PV/T-TW/Ti O_2 has the best eco-balance of a TE of 13.11 kg/yr. On average, PV/T-THVP1/Ti O_2 is the best configuration.

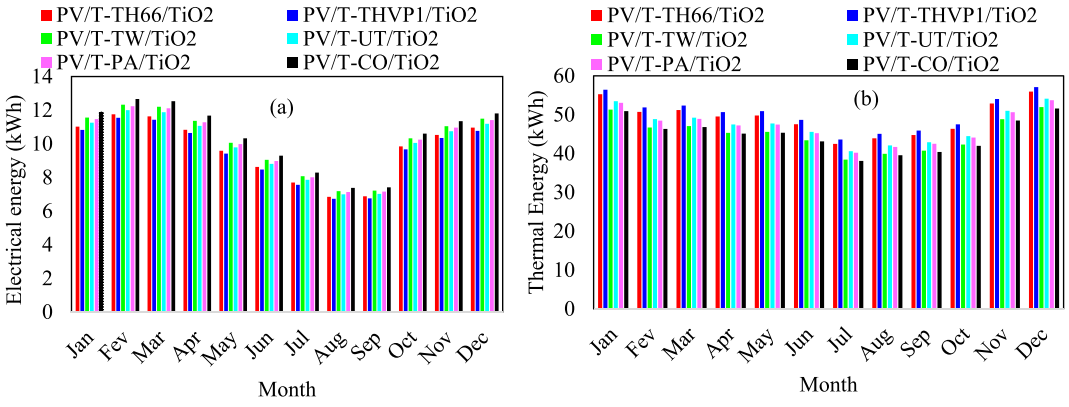

Fig. 18. Evaluation of electrical (a) and thermal (b) energy production in the MAROUA area.

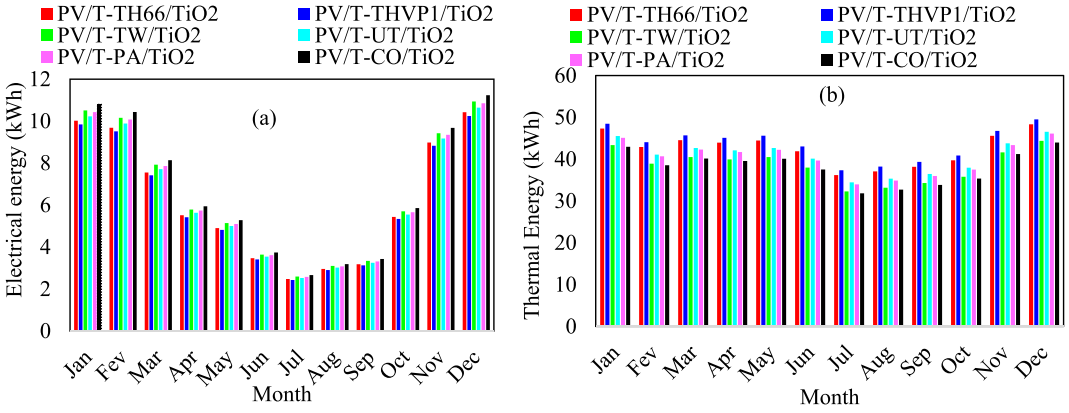

Fig. 19. Evaluation of electrical (a) and thermal (b) energy production in the NGAOUNDERE area.

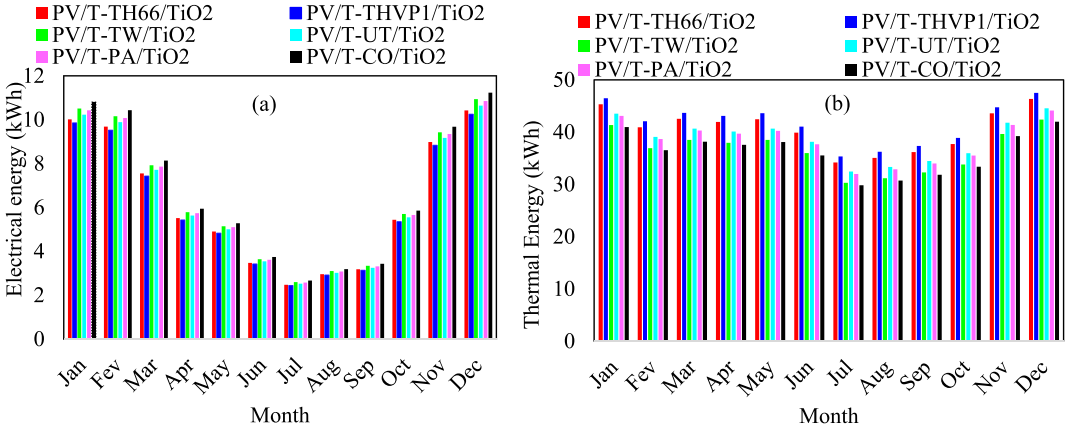

Fig. 20. Evaluation of electrical (a) and thermal (b) energy production in the DOUALA area.

In N'Gaoundéré, the PV/T-THVP1/Ti O_2 configuration is economically good with a CPBT of around 5 years and 2 months but PV/T-TW/Ti O_2 has the best eco-balance of a TE of 9.80 kg/yr. On average, PV/T-THVP1/Ti O_2 is the best configuration.

In Douala, the PV/T-THVP1/Ti O_2 configuration is economically good with a CPBT of around 5 years and 10 months but PV/T-CO/Ti O_2 has the best eco-balance of a TE of 7.45 kg/yr. On average, PV/T-THVP1/Ti O_2 is the best configuration.

In Bafoussam, the PV/T-THVP1/Ti O_2 configuration is economically good with a CPBT of around 5 years and 9 months but PV/T-TW/Ti O_2 has the best eco-balance of a TE of 8.15 kg/yr. On average, PV/T-UW/Ti O_2 is the best configuration.

Table 10 supports the analyzes in Table 9 and specifies in detail the classification of PV/T configurations according to the decision

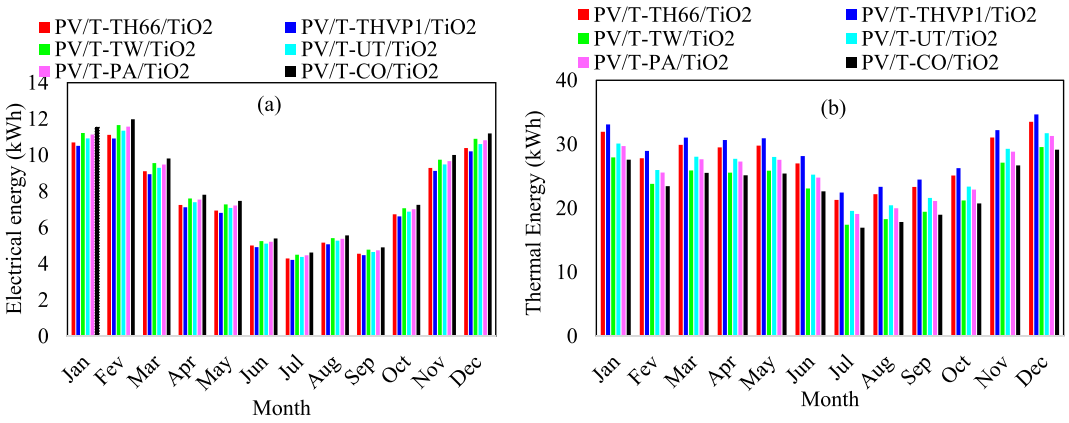

Fig. 21. Evaluation of electrical (a) and thermal (b) energy production in the BAFOUSSAM area.

parameters and according to the climatic zones. The PV/T-THVP1/Ti O_2 and PV/T-UW/Ti O_2 systems have an identical rank sum in the DOUALA, MAROUA and NGAOUNDERE zones. Priority is given to the smallest COE and NPV in order to choose a very economical system accessible to the population. The PV/T- THVP1/Ti O_2 system is therefore chosen and this mainly comes from the very high thermal energy produced with this configuration.

7.3.2. Economic benefit

PV/T systems based on vegetable oils are economically profitable despite their increased electricity consumption with pumping, they are produced locally. The initial costs of synthetic oils being a little higher because production is not local. The different COEs of all the PV/T configurations offered are between 21 and 33 % lower than the unit price per kilowatt of electricity in Cameroon.

7.3.3. Environmental benefit

The configuration most respecting environmental standards is observed in the YAOUNDE area with the PV/T-CO/system TiO_2 which presents the lowest emission rate of CO_2 6.95 kg per year. In general, synthetic oils have the highest carbon dioxide emissions in any area. This is certainly due to their composition of diphenyl oxide ($C_{13}H_{10}O$) which is a petroleum derivative. So, a slightly higher rate is recorded in the MAROUA area particularly with synthetic oils of 13.68 and 13.81 kg for TH66 and TVP1 respectively. However, it should be noted that these emissions are very low compared to the emissions CO_2 generated by other renewable energy systems.

Fig. 22 illustrates the different average scores achieved by each configuration. It is seen that, overall, the gap between the PV/T configurations with untreated water and therminolVP-1 oil is not very far compared to the others. The PV/T-THVP1/ TiO_2 is separated by 0.4 points from the PV/T-UW/system TiO_2, by 4.4 points from the PV/T-TW/system, by 10.4 points from the TiO_2 PV/T-TH66/TiO_2 system, by 13 points from the system PV/T-PA/TiO_2 and 16.8 of the PV/T-CO/ TiO_2 system. Comparison of the different configurations with those from the literature in Table 11 indicates a fairly good approximation, notably with a lower COE and TE.

8. Conclusion

In the present work, a numerical evaluation of a hybrid solar PV/T-NF system based on vegetable and synthetic oils is carried out. The comparative study is carried out with six (6) configurations of HTFs. A decision-making criterion through multi-objective optimization with seven functions including COE, NPV, TE, SI, AV, TAC and CPBT based on techno-economic and environmental analysis is carried out in five climatic zones. The most relevant conclusions of the study are.

- The addition of nanoparticles TiO_2 has more thermal influence in PV/T-TH66, PV/T-CO , PV/T-PA , PV/T-THVP1 systems respectively than in PV/T-TW and PV/T-UW systems;
- The sensitivity of nanoparticle morphology TiO_2 revealed that lamellar and spherical shapes increase the convective transfer coefficient between nanofluids and tubes;
- The thermal efficiency of the system improved with the volume concentration of the nanoparticles up to an average threshold of 4 % at 850 W/ m^2 where it tends to be constant after this value;
- Systems operating with treated and untreated water have better thermal efficiency, compared to systems with vegetable and synthetic oils which have high melting and boiling points allowing them to be more efficient at very high temperatures and d avoid coagulation;
- Alternatives that favor electrical energy production tend to have lower thermal energy production;
- The greatest improvement in electrical efficiency is with the PV/T-CO/configuration TiO_2;
- The annual evaluation of each configuration reveals that the PV/T systems with synthetic oils have good thermal production in hot zones and the PV/T-CO/TiO_2, PV/T-TW/ TiO_2 and PV/T-PA/ TiO_2 systems have led to the highest respective electricity production of 125.21 kWh/yr, 121.91 kWh/yr and 120.97 kWh/yr in the city of MAROUA;

Table 9
Values of optimal decision-making parameters by zone.

Area	Settings	COE ($/kWh)	NPV ($)	TE (kg/yr)	SI	TAC ($)	CPBT (years)
	PV/T-TH66/TiO_2	0.0363	666.3627	7.6181	1.2581	6.9253	5.6488
	PV/T-THVP1/TiO_2	0.0075	760,1068	7.7965	1.2852	1.4813	5.6248
	PV/T-TW/TiO_2	0.0093	649.1828	6.9747	1.2574	1.6355	5.7980
	PV/T-UW/TiO_2	0.0089	695.1252	7.3218	1.3467	1.6393	5.7188
	PV/T-PA/TiO_2	0.0731	538.2410	7.2805	1.2322	13.3151	5.7147
YAOUNDE	PV/T-CO/TiO_2	0.0860	472.3876	6.9516	1.1778	14.9497	5.7975
	PV/T-TH66/TiO_2	0.0318	1148.1913	13.6856	2.4163	10.9136	5.9946
	PV/T-THVP1/TiO_2	0.0053	1286.0070	13.8199	2.6398	1.8422	5.9996
	PV/T-TW/TiO_2	0.0063	1163.7846	13.1175	2.4836	2.0723	6.1979
	PV/T-UW/TiO_2	0.0062	1211,1358	13.3914	3.3133	2.0807	6.1126
	PV/T-PA/TiO_2	0.0635	970.1595	13.4304	2.2031	21.3412	6.0304
MAROUA	PV/T-CO/TiO_2	0.0728	891.70779	13.1968	1.9374	24.0240	6.1078
	PV/T-TH66/TiO_2	0.0300	1283.4071	10.3802	2.1563	7.7955	5.2549
	PV/T-THVP1/TiO_2	0.0063	1386.3555	10.5365	2.2632	1.6660	5.2345
	PV/T-TW/TiO_2	0.0075	1233.8955	9.8019	2.1894	1.8395	5.4005
	PV/T-UW/TiO_2	0.0072	1297.5626	10.1134	2.5399	1.8438	5.3259
	PV/T-PA/TiO_2	0.0594	1138.0121	10.0956	2.0459	15.0054	5.3142
NGAOUNDERE	PV/T-CO/TiO_2	0.0686	1055,1450	9.8127	1.8951	16.8527	5.3909
	PV/T-TH66/TiO_2	0.0189	652.8976	8.1216	2.0132	3.8412	5.9028
	PV/T-THVP1/TiO_2	0.0062	708,1003	8.3000	2.0781	1.2978	5.8757
	PV/T-TW/TiO_2	0.0072	612.0613	7.4694	2.0281	1.3557	6.0387
	PV/T-UW/TiO_2	0.0069	651.7967	7.8157	2.1880	1.3568	5.9651
	PV/T-PA/TiO_2	0.0363	568.4911	7.7810	1.9528	7.0772	5.9706
DOUALA	PV/T-CO/TiO_2	0.0424	518.4572	7.4555	1.8658	7.9184	6.0488
	PV/T-TH66/TiO_2	0.0512	854.6142	8.7460	2.3687	11.2055	5.8447
	PV/T-THVP1/TiO_2	0.0087	993.7657	8.8993	2.5685	1.9369	5.8121
	PV/T-TW/TiO_2	0.0107	837.0777	8.1508	2.4292	2.1827	6.1473
	PV/T-UW/TiO_2	0.0103	899.5048	8.4524	3.1533	2.1911	5.9975
	PV/T-PA/TiO_2	0.1032	668.9777	8.4587	2.1753	21.8422	5.9543
BAFOUSSAM	PV/T-CO/TiO_2	0.1200	577.1422	8.1871	1.9303	24.5720	6.1034

- The cooling systems used here show an improvement of up to 56.2 % on the energy produced and 12.08 % on the electrical efficiency of the hybrid PV/T system compared to uncooled PV with a COE between 0.0053 and 0.12, very below the unit price of electricity in the area;
- The decision-making evaluation of the objective functions noted a saving of $0.0075/kWh for the COE and NPV of $760.10 in YAOUNDE, $0.0053/kWh for the COE and NPV of $1286 in MAROUA
- 0.0063$ of COE and 1386.35$ of NPV in NGAOUNDERE, 0.0087$ of COE and 993.76$ of NPV in BAFOUSSAM for the PV/T-THVP-1/ TiO_2 system, 0.0069$ of COE and 651.79$ of NPV in DOUALA for the system PV/T-UW/ TiO_2 which are the best configurations.
- In terms of electrical efficiency, the cotton/ TiO_2 configuration is better, in terms of electrical energy cost, therminolVP-1/ TiO_2 is better;
- From an environmental point of view, configurations with vegetable oils tend more towards zero carbon than the use of synthetic oils. On the other hand, they are less durable;
- From an economic point of view, solar PV/T systems with synthetic oils are more economical than those with vegetable oils. But the average scores allowed us to deduce that they can all be good alternatives to water.

These results could be exploited by solar industries in the design of solar collectors for the adoption of a conventional cooling system and also in decision-making. Taking into account local energy consumption and demand in the study could be necessary in the

Table 10
Rank of different configurations.

Area	Settings	R_{COE}	R_{NPV}	R_{TE}	R_{SI}	R_{TAC}	R_{CPBT}	R_{AV}	R_{sum}
YAOUNDE	PV/T-TH66/TiO_2	4	3	5	3	4	2	5	26
	PV/T-THVP1/TiO_2	1	1	6	2	1	1	6	18
	PV/T-TW/TiO_2	3	4	2	4	2	6	2	23
	PV/T-UW/TiO_2	2	2	4	1	3	4	1	17
	PV/T-PA/TiO_2	5	5	3	5	5	3	3	29
	PV/T-CO/TiO_2	6	6	1	6	6	5	4	34
MAROUA	PV/T-TH66/TiO_2	4	4	5	4	4	1	6	28
	PV/T-THVP1/TiO_2	1	1	6	2	1	2	5	18
	PV/T-TW/TiO_2	3	3	1	3	2	6	3	21
	PV/T-UW/TiO_2	2	2	3	1	3	5	2	18
	PV/T-PA/TiO_2	5	5	4	5	5	3	4	31
	PV/T-CO/TiO_2	6	6	2	6	6	4	1	31
NGAOUNDERE	PV/T-TH66/TiO_2	4	3	5	4	4	2	6	28
	PV/T-THVP1/TiO_2	1	1	6	2	1	1	5	17
	PV/T-TW/TiO_2	3	4	1	3	2	6	2	21
	PV/T-UW/TiO_2	2	2	4	1	3	4	1	17
	PV/T-PA/TiO_2	5	5	3	5	5	3	4	30
	PV/T-CO/TiO_2	6	6	2	6	6	5	3	34
DOUALA	PV/T-TH66/TiO_2	4	2	5	4	4	2	6	27
	PV/T-THVP1/TiO_2	1	1	6	2	1	1	5	17
	PV/T-TW/TiO_2	3	4	2	3	2	5	2	21
	PV/T-UW/TiO_2	2	3	4	1	3	3	1	17
	PV/T-PA/TiO_2	5	5	3	5	5	4	3	30
	PV/T-CO/TiO_2	6	6	1	6	6	6	4	35
BAFOUSSAM	PV/T-TH66/TiO_2	4	3	5	4	4	2	6	28
	PV/T-THVP1/TiO_2	1	1	6	2	1	1	5	17
	PV/T-TW/TiO_2	3	4	1	3	2	6	2	21
	PV/T-UW/TiO_2	2	2	3	1	3	4	1	16
	PV/T-PA/TiO_2	5	5	4	5	5	3	3	30
	PV/T-CO/TiO_2	6	6	2	6	6	5	4	35

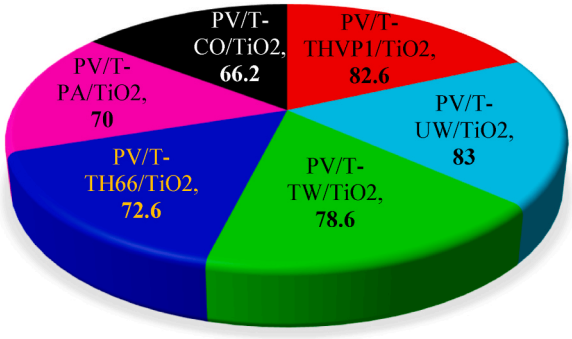

Fig. 22. Average score of each configuration.

Table 11
Comparison of the best configurations of hybrid PV/T systems.

Studies	Solar systems	Electrical efficiency (%)	Thermal efficiency (%)	Optimization methods	COE ($/kWh)	NPV ($)	TE (kg)	IF	CPBT (years)
Present study	PV/T-THVP1/ TiO_2	12.99	71.29	MOO	0.007	760.10	7.79	1.28	5.62
Present study	PV/T-UW/ TiO_2	13.28	76.82	MOO	0.008	695.12	7.32	1.34	5.71
Present study	PV/T-PA/ TiO_2	12.59	72.2	MOO	0.036	568.49	7.78	1.95	5.97
Present study	PV/T-CO/ TiO_2	13.42	71.52	MOO	0.042	518.45	7.45	1.86	6.04
Ref [5]	PV/T-Water	12.3	–	EXP	0.044	–	–	–	2.48
Ref [17]	PV/TW/ TiO_2	14.56	45.95	AHP	–	–	–	–	5.61
Ref [17]	PV/TW/ Al_2O_3	14.34	38.78	AHP	–	–	–	–	5.93
Ref [31]	PV/TW/ Al_2O_3	13.4	65	–		–	–	–	8.5
Ref [32]	PV/T-UW/Ag	14.0	60.8	CFDs	0.002	–	–	–	1983
Ref [33]	PV/T-TW/ Al_2O_3	17.1	–	–	–	–	–	–	12
Ref [47]	PV/T-Air	13.16	23.34	TOPSIS	0.015	407.43	72.11	1.162	4.95

case of pre-sizing of these systems.

Funding statement

This research did not receive any specific grant from funding agencies in the public, commercial, or not-for-profit sectors.

Data availability statement

We have included the data sources in the manuscript.

CRediT authorship contribution statement

Armel Zambou Kenfack: Writing - review & editing, Writing - original draft, Visualization, Validation, Supervision, Software, Resources, Project administration, Methodology, Investigation, Funding acquisition, Formal analysis, Data curation, Conceptualization. **Modeste Kameni Nematchoua:** Visualization, Validation, Methodology, Conceptualization. **Elie Simo:** Visualization, Validation, Supervision, Methodology, Conceptualization. **Franck Armel Talla Konchou:** Validation, Supervision, Methodology, Investigation. **Mahamat Hassane Babikir:** Supervision. **Boris Abeli Pekarou Pemi:** Writing - original draft, Methodology. **Venant Sorel Chara-Dackou:** Writing - review & editing, Writing - original draft, Visualization, Validation, Supervision, Methodology, Conceptualization.

Declaration of competing interest

The authors declare that they have no known competing financial interests or personal relationships that could have appeared to influence the work reported in this paper.

Abbreviations

AHP	analytical hierarchy process decision
AV	Availablity
COE	Cost of Energy
CPBT	Temps de retour sur investissement
CRF	Facteur de récupération
EXP	Experimental
MOO	Multi-ojective optimzation
MAE	Mean absolute error
NF	nanofluids
NPC	Net present values
NP	Nanoparticule
TE	Emission rate
TOPSIS	Technique for Order Preference by Similarity to Ideal Solution
TH66	Therminol66 oil
THVP1	TherminolVP-1 oil
TW	Treated water
TAC	Total annuel cost
TC	Thermal collector
UW	Untreated water
PA	Palm oil
PV/T	Photovoltaic/thermal
CO	Cotton oil

Nomenclature

A	Surface, m^2
C	Specific heat, J $kg^{-1}K^{-1}$
D	Diameter, m
d	Diamètre de l'atome
G	Solar radiation, W/ m^{-2}
h	Heat transfer coefficient, W/ m^2K
L	Length, m
L	Largeur du nanowire
M	Mass, kg
$\dot{m}$	Mass flow rate, kg/m^3
E_x	Exergy
T	Temperature, °C
t	Time, h
Ra	Rayleigh number
N_u	Nusselt number
N	Number of tubes
h	Largeur du nanofilm
W	Spacing of tubes, m
σ	Stephan Bolzmann constant W/ $m^{-2}K^{-4}$

Subscripts

a	ambiant
C	convection
Bf	basefluid
cond	conduction
ex	exergy
O	out
F	fluid
pv	PV module
p	Absorber plate
r	Radiation
i	Insulation
el	electrical
th	thermal
nf	nanofluid
t	tube

s	Sun
Greek symbols	
α	Absorbtivity
η	Efficiency
β	Angle of inclination
ρ	density
$\beta^{'}$	Volumetric coefficient of expansion
τ	Transmissivity
δ	Thickness
φ	Volume concentartion
ε	Emissivity

References

[1] F.N. Nasse, M.K.D. Boris, H.D. Grisseur, G.F.N. Cherelle, J.T. Kewir, T. Martin, Contribution of the mix renewable energy potentials in delivering parts of the electric energy needs in the west region of Cameroon, Heliyon 9 (2023) 14554, https://doi.org/10.1016/j.heliyon.2023.e14554.

[2] T.D. Nzoko, K.F.A. Talla, T.H. Djeudjo, K.C.V. Aloyem, R. Tchinda, Optimization of Short-Term Forecast of Electric Power Demand in the city of Yaoundé-Cameroon by a hybrid model based on the combination of neural networks and econometric methods from a designed energy optimization algorithm, Technol. Forecast. Soc. Change 187 (2023) 122212, https://doi.org/10.1016/j.techfore.2022.122212.

[3] I. Chu Donatus, S. Guy Clarence, A. Roger Houèchénè, Optimum site selection of hybrid solar photovoltaic (PV) - hydro power plants in off grid locations in Cameroon using the multi-criteria decision analysis (MCDA), energy sources , Part A: recovery, utilization, and Environmental Effects 45 (3) (2023) 8076–8091, https://doi.org/10.1080/15567036.2023.2224739.

[4] S. Mohammad, M. Passandideh-Fard, Experimental and numerical study of metal-oxides/water nanofluids as coolant in photovoltaic thermal systems (PVT), Sol. Energy Mater. Sol. Cell. 157 (2016) 533–542, https://doi.org/10.1016/j.solmat.2016.07.008.

[5] P. Seepana, B.A. Ephraim, Ak, I.V. Vladimir, Thermo-enviro-economic analysis of solar photovoltaic/thermal system incorporated with u-shaped grid copper pipe, thermal electric generators and nanofluids: an experimental investigation, J. Energy Storage 60 (2023) 106611, https://doi.org/10.1016/j.est.2023.106611.

[6] M. Du, G.H. Tang, T.M. Wang, Exergy analysis of a hybrid PV/T system based on plasmonic nanofuids and silica aerogel glazing, Sol. Energy 183 (2019) 501–511, https://doi.org/10.1016/j.solener.2019.03.057.

[7] A.H.A. AlWaeli, M.T. Chaichan, K. Sopian, H.A. Kazem, Influence of the base fluid on the thermo-physical properties of PV/T nanofluids with surfactant, Case Stud. Therm. Eng. 13 (2019) 100340, https://doi.org/10.1002/er.4442.

[8] H. Farzad, Md Rezwanul K, A.B. Arafat, A review on recent advancements of the use of nano fluid in hybrid photovoltaic/thermal (PV/T) solar systems (2020), https://doi.org/10.1016/j.renene.2022.01.116.

[9] K. Zakariya, U.R. Ateekh, Selection of a photovoltaic panel cooling technique using multi-criteria decision analysis, Appl. Sci. 13 (3) (2023), https://doi.org/10.3390/app13031949, 1949, (February).

[10] K. Waldemar, C. Katarzyna, Energy and exergy analysis of photovoltaic panels in northern Poland, Renew. Sustain. Energy Rev. 174 (January 2023) 113138, https://doi.org/10.1016/j.rser.2022.113138.

[11] M.H. Omar, R.A. Omar, Badran MS Performance analysis of hybrid photovoltaic thermal solar system in Iraq climate condition, Therm. Sci. Eng. Prog. 17 (2020) 100359, https://doi.org/10.1016/j.tsep.2019.100359. ISSN 2451-9049.

[12] R.K. Mishra, G.N. Tiwari, Energy and exergy analysis of hybrid photovoltaic thermal water collector for constant collection temperature mode, Sol. Energy 90 (2013) 58–67, https://doi.org/10.1016/j.solener.2012.12.022. ISSN 0038-092X.

[13] M.A. Omar, R.A. Omar, I.M. Shaaban, Technical, economical and environmental feasibility study of a photovoltaic system under the climatic condition of north Iraq, Int. J. Ambient Energy 44 (1) (2023) 212–220, https://doi.org/10.1080/01430750.2022.2126004.

[14] R.A. Omar, M.A. Omar, M.A. Bashar, S.Q. Veen, Obed MA Energy, exergy, economical and environmental analysis of photovoltaic solar panel for fixed, single and dual axis tracking systems: an experimental and theoretical study, Case Stud. Therm. Eng. 51 (2023) 103635, https://doi.org/10.1016/j.csite.2023.103635. ISSN 2214-157X.

[15] A. Ibrahim, M.R. Ramadan, A.E.M. Khallaf, M. Abdulhamid, A comprehensive study for Al_2O_3 nanofluid cooling effect on the electrical and thermal properties of polycrystalline solar panels in outdoor conditions, Environ. Sci. Pollut. Control Ser. (2023) 1–22, https://doi.org/10.1007/s11356-023-25928-3.

[16] H.A. Sabhan, R.A. Omar, M.A. Omar, Energetic and exegetic performance analysis of platelets plate solar collector under variables heat transfer coefficient and inlet water temperature, Case Stud. Therm. Eng. 28 (2021) 101700, https://doi.org/10.1016/j.csite.2021.101700. ISSN 2214-157X.

[17] A. Sohani, S. Hassan, H. Sayyaadi, S. Samiezadeh, M Hossein D, N. Sandro, K. Nader, Selecting the best nanofluid type for A photovoltaic thermal (PV/T) system based on reliability, efficiency, energy, economic, and environmental criteria, J. Taiwan Inst. Chem. Eng. 124 (2021) 351–358. July, https://doi://10.1016/j.jtice.2021.02.027.

[18] Talib KM Effect of using Al2O3/TiO2 hybrid nanofluids on improving the photovoltaic performance, Case Stud. Therm. Eng. 47 (2023) 103112, https://doi.org/10.1016/j.csite.2023.103112. ISSN 2214-157X.

[19] B.K. Talha, G. Aytac, R. Ahmed, Numerical and experimental study of a PVT water system under daily weather conditions, Energies, September 15 (18) (2022) 6538, https://doi.org/10.3390/en15186538.

[20] H. Ahmed, E. Abdelgalil, M.E. Hesham, Experimental and numerical investigation for PV cooling by forced convection, Alex. Eng. J. 64 (2023) 427–440, https://doi.org/10.1016/j.aej.2022.09.006 (February).

[21] M. Mourshed, Masuk Ni, H.Q. Nguyen, B. Shabani, An experimental approach to energy and exergy analyzes of a hybrid PV/T system with simultaneous water and air cooling, Energies 15 (18) (2022) 6764, https://doi.org/10.3390/en15186764.

[22] C. Narendra, R. Easwaramoorthi, K. Suresh, M. Sudhanshu, K. Anil, S. Shanmugasundaram, Quantum-sized TiO2 particles as highly stable super-hydrophilic and self-cleaning antisoiling coating for photovoltaic application, Sol. Energy 258 (2023) 194–202, https://doi.org/10.1016/j.solener.2023.04.062. ISSN 0038-092X.

[23] K.A. Zambou, N.M. Kameni, E. Simo, M.N. Mfoundikou, F.J.V. Kenfack, M.H. Babikir, V.S. Chara-Dackou, Exergetic Optimization of Some Design Parameters of the Hybrid Photovoltaic/thermal Collector with Bi-fluid Air/ternary Nanofluid (CuO/MgO/TiO2), vol. 5, Springer Nature Applied Sciences, 2023, p. 226, https://doi.org/10.1007/s42452-023-05455-z.

[24] M.I. Hussain, K. Jun-Tae, Sustainability performance evaluation of photovoltaic/thermal (PV/T) system using different design configurations, Sustainability 12 (2020), https://doi.org/10.3390/su12229520, 22-9520.

[25] J.F. Hoffmann, J.F. Henry, G. Vaitilingom, R. Olives, M. Chirtoc, D. Caron, X. Py, Temperature dependence of thermal conductivity of vegetable oils for use in concentrated solar power plants, measured by 3omega hot wire method, Int. J. Therm. Sci. 107 (2016) 105–110, https://doi.org/10.1016/j.ijthermalsci.2016.04.002.

[26] V.S. Chara-Dackou, D. Njomo, R. Tchinda, M.H. Babikir, Y.S. Kondji, Thermal performance analysis of the parabolic trough solar collector in the sub-Saharan climate of the Central African Republic, Sustain. Energy Technol. Assessments 58 (2023) 103331, https://doi.org/10.1016/j.seta.2023.103331.
[27] R. Fazlay, H. Khairul, R. Saidur, A. Navid, M. Syed, D. Likhan, Performance optimization of a hybrid PV/T solar system using Soybean oil/Mxene nanofluids as A new class of heat transfer fluids, Sol. Energy 208 (2020) 124–138, https://doi.org/10.1016/j.solener.2020.07.060. July.
[28] V.W. Vignesh, R. Munirah, Z.A. Mohd, Thermophysical properties of vegetable oil-based hybrid nanofluids containing Al2O3-TiO2 nanoparticles as insulation oil for power transformers, Nanomaterials 12 (2022) 3621, https://doi.org/10.3390/nano12203621.
[29] M.A. Ehyaei, A. Ahmadi, M. El Haj Assad, A.A. Hachicha, Z. Said, Energy, exergy and economic analyzes for the selection of working fluid and metal oxide nanofluids in a parabolic trough collector, Sol. Energy 187 (2019) 175–184, https://doi.org/10.1016/j.solener.2019.05.046.
[30] H. Samir, R. Saidur, M. Saad, R.A. Taylor, Environmental and exergy benefit of nanofluid-based hybrid PV/T systems, Energy Convers. Manag. 123 (2016) 431–444, https://doi.org/10.1016/j.enconman.2016.06.061. September.
[31] M.I. Hussain, K. Jun-Tae, Conventional fluid- and nanofluid-based photovoltaic thermal (PV/T) systems: a technoeconomic and environmental analysis, Int. J. Green Energy (2018) 1543–5075, https://doi.org/10.1080/15435075.2018.1525558.
[32] O.L. Muhammad, Z.S. Ahmet, Design, performance and economic analysis of a nanofluid-based photovoltaic/thermal system for residential applications, Energy Convers. Manag. 149 (2017) 467–484, https://doi.org/10.1016/j.enconman.2017.07.045.
[33] S. Abdo, H. Saidani-Scott, Effect of using saturated hydrogel beads with alumina water-based nanofluid for cooling solar panels: experimental study with economic analysis, Sol. Energy 217 (2021) 155–164, https://doi.org/10.1016/j.solener.2021.01.050, elsevier, February.
[34] G. Rongoumi, S. Adamou, Y. Nadjilom, D. Gomoung, T. Toukam, A. Ngakou, Morpho-physiological and biochemical characterization of soybean-associated rhizobia and effect of their liquid inoculant formulation on nodulation of host plants in the Cameroon cotton fields zone, Am. J. Plant Sci. 14 (2023) 812–827, https://doi.org/10.4236/ajps.2023.147054.
[35] N.A. Ada, M.A. Lacour, N.E. Benis, Greenhouse gas emissions along the value chain in palm oil producing systems: a case study of Cameroon, Cleaner and Circular Bioeconomy 6 (2023) 100057, https://doi.org/10.1016/j.clcb.2023.100057.
[36] Y. Khanjari, F. Pourfayaz, A.B. Kasaeian, Numerical investigation on using of nanofluid in a water-cooled photovoltaic thermal system, Energy Convers. Manag. 122 (2016) 263–278, https://doi.org/10.1016/j.enconman.2016.05.083.
[37] S.E.B. Maiga, S.J. Palm, C.T. Nguyen, G. Roy, N. Galanis, Heat transfer enhancement by using nanofluids in forced convection flows, Int. J. Heat Fluid Flow 26 (4) (2005) 530–546, https://doi.org/10.1016/j.ijheatfluidflow.2005.02.004.
[38] S. Madan, L. Sekhants'o, T. Spirit, Effects of size and shape on the specific heat, melting entropy and enthalpy of nanomaterials, J. Taibah Univ. Sci. 11 (6) (2017) 922–929, https://doi.org/10.1016/j.jtusci.2016.09.011.
[39] B. Mehdi, M. Ali, M. Hossein, Second law assessment of nanofluid flow in a channel fitted with conical ribs for utilization in solar thermal applications: effect of nanoparticle shape, Int. J. Heat Mass Tran. 151 (2020) 119387, https://doi.org/10.1016/j.ijheatmasstransfer.2020.119387.
[40] M.H. Mosarof, M.A. Kalam, H.H. Masjuki, A.M. Ashraful, M.M. Rashed, H.K. Imdadul, I.M. Monirul, Implementation of palm biodiesel based on economic aspects, performance, emission, and wear characteristics, Energy Convers. Manag. 105 (2015) 617–629, https://doi.org/10.1016/j.enconman.2015.08.020.
[41] K.G.T. Hollands, T.E. Unny, G.D. Raithby, L. Konicek, Free convection heat transfer across inclined air layers, Trans. ASME J.Heat Transf. 98 (1976) 189–193, https://doi.org/10.1115/1.3450517.
[42] B. Sujala, O. Jae-Heun, E. Seung-Hee, K.K. Gopi, H.K. Dae, Simulation and model validation of sheet and tube type photovoltaic thermal solar system and conventional solar collecting system in transient states, Sol. Energy Mater. Sol. Cell. (103) (2012) 184–193, https://doi.org/10.1016/j.solmat.2012.04.017.
[43] B.H. Truong, P. Nallagownden, K.H. Truong, R. Kannan, D.N. Vo, N. Ho, Multi-objective search group algorithm for thermo-economic optimization of platelets-plate solar collector, Neural Comput. Appl. (2021) 1–27, https://doi.org/10.1007/s00521-021-05915-w.
[44] H. Adun, A. Michael, D. Mustafa, B. Olusola, S. Mehmet, K. Ravinder, A numerical and exergy analysis of the effect of ternary nanofluid on performance of Photovoltaic thermal collector, J. Therm. Anal. Calorim. 145 (2021) 1413–1429, https://doi.org/10.1007/s10973-021-10575-y.
[45] H.B. Mahamat, D. Njomo, B. Mahamat, V.S. Chara-Dackou, S.K. Yvon, Y.K. Mahamoud, Thermal modeling of a parabolic trough collector in a quasi-steady state regime, J. Renew. Sustain. Energy 13 (2021) 013703, https://doi.org/10.1063/1.5145272.
[46] A.S. Abdelrazik, R. Saidur, Al-Sulaiman, FA Insights on the thermal potential of a state-of-the-art palm oil/MXene nanofluid in a circular pipe, J. Therm. Anal. Calorim. 148 (3) (2023) 913–926, https://doi.org/10.1007/s10973-022-11795-6.
[47] A.J. Cetina-Quinones, I. Polanco-Ortiz, M.A. Pedro, J.G. Hernandez-Perez, A. Bassam, Innovative heat dissipation design incorporated into a solar photovoltaic thermal (PV/T) air collector: an optimization approach based on 9E analysis, Therm. Sci. Eng. Prog. (2023) 2451–9049, https://doi.org/10.1016/j.tsep.2022.101635, 38:101635.
[48] T.H. Djeudjo, D. Njomo, K.F.A. Talla, R. Tchinda, Techno-economic and environmental feasibility study with demand-side management of photovoltaic/wind/hydroelectricity/battery/diesel: a case study in Sub-Saharan Africa, Energy Convers. Manag. 258 (2022) 196–8904, https://doi.org/10.1016/j.enconman.2022.115494.
[49] V.S. Chara-Dackou, D. Njomo, H. Babikir, N. Mbouombouo, G. Pofoura, R. Tchinda, Processing sunshine duration measurements for assessment of solar radiation in climatic regions of the Central African Republic, J. Sol. Energy Eng. 144 (2022) 1–15, https://doi.org/10.1115/1.4053483.
[50] H. Wei, Z. Yang, J. Jie, Comparative experiment study on photovoltaic and thermal solar system under natural circulation of water, Appl. Therm. Eng. (31) (2011) 3369–3376, https://doi.org/10.1016/j.applthermaleng.2011.06.021.
[51] A. Sajid, Z. Jinzhi, H. Atazaz, Y. Yanping, Y. Saima, S. Yafen, Z. Chao, Economic evaluation and annual performance analysis of a novel series-coupled PV/T and solar TC with solar direct expansion heat pump system: an experimental and numerical study, Renew. Energy 204 (2023) 400–420, https://doi.org/10.1016/j.renene.2023.01.032.
[52] Pvgis, Consulted February 5 (2023). https://re.jrc.ec.europa.eu/pvg_tools/fr/.